MOLECULAR AND CELLULAR BIOLOGY, June 1996, p. 3138–3155 Vol. 16, No. 6
0270-7306/96/$04.00+0

A Developmentally Modulated Chromatin Structure at the Mouse Immunoglobulin κ 3′ Enhancer

MARIA C. ROQUE, PATRICIA A. SMITH, AND VERONICA C. BLASQUEZ*

Department of Chemistry and Biochemistry, University of Notre Dame, Notre Dame, Indiana 46556

Received 18 July 1995/Returned for modification 15 September 1995/Accepted 19 March 1996

Transcription of the mouse immunoglobulin κ gene is controlled by two enhancers: the intronic enhancer (Ei) that occurs between the joining (Jκ) and constant (Cκ) exons and the 3′ enhancer (E3′) located 8.5 kb downstream of the gene. To understand the role of E3′ in the activation of the mouse immunoglobulin κ gene, we studied its chromatin structure in cultured B-cell lines arrested at various stages of differentiation. We found that 120 bp of the enhancer's transcriptional core becomes DNase I hypersensitive early in B-cell development. Genomic footprinting of pro-B and pre-B cells localized this chromatin alteration to B-cell-specific protections at the region including the direct repeat (DR) and the sequence downstream of the DR (DS), the PU.1–NFEM-5 site, and the core's E-box motif, identifying bound transcription factors prior to kappa gene rearrangement. Early footprints were, however, not detected at downstream sites proposed to play a negative role in transcription. The early chromatin structure persisted through the mature B-cell stage but underwent a dramatic shift in plasma cells, correlating with the loss of guanosine protection within the DR-DS junction and the appearance of novel footprints at a GC-rich motif upstream and the NF-E1 (YY1/δ)-binding site downstream. Gel shift analysis demonstrated that the DR-DS junction is bound by a factor with properties similar to those of BSAP (B-cell-specific activator protein). These results reveal developmental-stage-specific changes in the composition of nuclear factors bound to E3′, clarify the role of factors that bind constitutively in vitro, and point to the differentiation of mature B cells to plasma cells as an important transitional point in the function of this enhancer. The observed changes in nuclear factor composition were accompanied by the rearrangement of positioned nucleosomes that flank the core region, suggesting a role for both nuclear factors and chromatin structure in modulating κE3′ function during B-cell development. The functional implications of the observed chromatin alterations are discussed in the context of recent studies on κE3′ and the factors that bind to it.

B cells differentiate from hematopoietic stem cells through an ordered progression of molecular events marked by the rearrangement and expression of the immunoglobulin heavy (IgH)- and light (Igκ or Igλ)-chain genes (4, 27, 63). The earliest identifiable cells of the B lineage are the pro-B cells. These cells do not express immunoglobulin proteins but can be defined by the appearance of early cell surface markers (27, 63). Pro-B cells rearrange IgH gene segments D_H to J_H (19, 27, 30), but functional heavy-chain gene rearrangement (V_H to D_HJ_H) is not observed until the pre-B-cell stage, in which the μ heavy chain is first observed in the cytoplasm (4, 27). Light-chain gene rearrangement follows μ expression, resulting in the synthesis of κ or λ polypeptides and complete antibody assembly on the cell surface. This marks the immature B-cell (IgM^+) stage and, subsequently, the mature B-cell (IgM^+ IgD^+) stage. Antigen binding coupled with stimulatory signals from T cells triggers the differentiation of mature B cells into antibody-secreting cells, the terminal stage of B-cell differentiation. This final stage, also called the plasma cell stage, is characterized by high levels of immunoglobulin production boosted by accelerated rates of transcription of both heavy- and light-chain genes (15, 33, 77).

B-cell-specific enhancers play a key role in the activation and regulation of immunoglobulin gene transcription during development. These elements function by binding *trans*-acting nuclear factors. Transcription of the mouse immunoglobulin κ gene is controlled by two enhancers: the intronic enhancer (Ei), which is found between the joining (Jκ) and constant (Cκ) exons, and the 3′ enhancer (E3′), which is located 8.5 kb downstream of the gene (41, 56, 60). These enhancers exert tissue-specific and developmental-stage-specific transcriptional controls, being both inactive at the pre-B-cell stage and active at the B-cell and plasma cell stages (7, 35, 42, 57). While the function of Ei and the factors that bind to it have been well studied (reviewed in reference 67; see also references 8, 37, 43, 65, 69, 73, and 79), the role of the E3′ in kappa gene regulation has just begun to unfold.

Deletional analyses have localized most of the E3′ transcriptional activity to a core region of 132 bp (42, 57). Sequence elements within this minimal fragment have been shown to bind a number of transcription factors. Among these are the B-cell-specific complex composed of PU.1 and NF-EM5 (59) and the ubiquitously expressed E2A helix-loop-helix protein (E12/E47) which binds an E-box (CANNTG) sequence within the core region (31, 57; this E box will be referred to as E box 1 to distinguish it from other E boxes found in this enhancer). Factors that bind a direct repeat (DR) region and sequences just downstream (DS) to it have also been detected by in vivo footprinting of human κE3′ (31). The analogous DR region of mice was recently shown to bind cyclic AMP response element binding factors ATF-1 and CREM (58). Although most of these binding sites have been shown to contribute to enhancer function by transient expression assays (31, 42, 57–59), none of the DNA-binding activities has been shown to be developmentally regulated. In pre-B cells, negative control of E3′ function has been localized to sequences outside of the core region (53). DNA elements within this region bind the ubiquitous zinc

* Corresponding author. Phone: (219) 631-8353. Fax: (219) 631-6652.

finger protein NF-E1 (also known as YY1 or δ), lymphoid cell-specific factor LEF-1, and E12/E47-like factors which bind two other E boxes (E boxes 2 and 3) in this region (40, 53). Although NF-E1 has been shown to be capable of repression in transient expression assays (53), negative roles for LEF-1 and E12/E47 have not been demonstrated. Also, the ubiquitous nature of both NF-E1 and E12/E47 (28, 45, 53) is difficult to reconcile with a putative negative role at the pre-B-cell stage. It thus remains unclear which of these factors play a developmental role in the function of E3′.

Since access of protein factors to their recognition sites within the nucleus is influenced by the assembly of DNA into chromatin, a complete understanding of enhancer function must take chromatin structure into account. We utilized the techniques of chromatin analysis to investigate the in vivo state of protein-DNA interactions at mouse κE3′ during development. By using a rapid method of DNase I hypersensitivity analysis, we found that the core region of E3′ becomes highly susceptible to nuclease digestion prior to kappa gene rearrangement. This hypersensitive structure is detectable in pro-B cells and persists in pre-B and mature B cells but undergoes a dramatic transition in plasma cells. By using ligation-mediated PCR (LMPCR)-aided genomic footprinting, we localized these open chromatin regions to protected guanosine residues at the DR-DS region, the PU.1–NFEM-5 site, and the E box 1 motif in pro-B, pre-B, and mature B cells. No guanosine footprints were detected at the LEF-1, NF-E1, or E box 2 or 3 site at the pro- and pre-B-cell stages. Interestingly, the chromosomal transition at the plasma cell stage correlated with loss of guanosine protection within a subregion of the DR-DS region, the appearance of footprints at a region upstream and the NF-E1 site downstream of the core, and the rearrangement of positioned nucleosomes that flank the core region as gleaned from micrococcal nuclease (MNase) digestion analysis. Our results not only showed that transcription factors bind κE3′ prior to kappa gene rearrangement but also identified sites that bind nuclear factors in a developmentally regulated fashion. We found that one of these developmental sites binds a factor with properties similar to those of BSAP (B-cell-specific activator protein) (9). Since some of the other factors bind κE3′ constitutively in vitro, we suggest a role for both nuclear factors and chromatin structure in modulating κE3′ function during B-cell development.

TABLE 1. Genotypes, immunoglobulin expression, and chromatin structures of cell lines used in this study[a]

Cell line	Genotype			Immunoglobulin expression	Relative κ mRNA level	HSS at κE3′	Reference(s)
	H	κ	λ				
Pro-B and pre-B cells							
LyD9	G	G	G	−	−	−	52
BASC6C2	R	G		−	−	+, E	30
26-4 BAMC1	R	G		−	ND	+, E	30
HAFTL1	R	G		−	−	+, E	19
38B9	R	G		−	−	+, E	3
18-81Y	R	G		μ+	−	+, E	3, 5
300-19P-S20	R	G		ND	−	+, E	62
Pre-B–mature B cells							
P4-11	R	R		Dμ+, κ+	1	+, E	62
P8	R	R		μ+, κ+	ND	+, E	62
Mature B cells							
BALB-1427	R	R		μ+, κ+	25	+, E	48
WEHI 231	R	R		μ+, κ+	286	+, E	6
BCL1	R	R	R	μ+, λ+	45	+, E	14
Plasma cells							
S194	R	R		α+, κ+	4,800	+, L	6
MPC11	R	R		γ2b, κ+	8,250	+, L	6
J558	R	R	R	α+, λ+	1,500	+, L	6
HNK-1 (hybridoma)	R	R		μ+, κ+	ND	+, L	6
P3X63Ag8.653	R	R			ND	+, L	6
EL4 T cells	G	G	G	−	−	−	6
P388D1 macrophages	R	R	R	−	−	−	6
Nonhematopoietic L cells (fibroblasts)	G	G	G	−	−	−	6

[a] The genotypes and immunoglobulin expression phenotypes were obtained from the references listed or from our own studies. Genotype is abbreviated as G (germ line) or R (rearranged) for the heavy-chain gene (H), kappa light-chain gene (κ), and lambda light-chain gene (λ). Immunoglobulin expression is reported as + for the presence or − for the absence of a specific immunoglobulin protein. μ, γ2b, or α refers to the heavy-chain isotype, while κ or λ refers to the light-chain class. Relative κ mRNA numerical values were obtained by normalizing densitometric scans of κ mRNA bands from a Northern blot with respect to actin mRNA and comparing the ratio with P4-11, which was arbitrarily assigned a value of 1. A minus sign indicates the absence of κ mRNA, while ND means not determined. The presence (+) or absence (−) of E and L refer to early and late hypersensitivity patterns, respectively (see text).

MATERIALS AND METHODS

Cell lines. The genotypes and phenotypes of the cell lines used in this study are listed in Table 1. The sources of the cell lines are as follows: LyD9 is from T. Kinashi (Boston, Mass.) with permission from R. Palacios (Basel Institute of Immunology); BASC6C2 and 26-4 BAMC1 are from J. Pierce (National Institutes of Health); HAFTL1 is from M. Xu at S. Tonegawa's laboratory (Massachusetts Institute of Technology); 38B9 is from D. Baltimore (Massachusetts Institute of Technology); 18-81Y is from N. Rosenberg (Tufts University); 300-19P-S20 is a subclone of 300-19P obtained from F. Alt (Harvard University); P4-11 and P-8 are from M. Reth (Freiburg, Germany); BALB1427 is from H. Morse (National Institutes of Health); BCL1 is from P. Tucker (University of Texas Southwestern Medical Center) and the American Type Culture Collection; and WEHI231, S194, MPC11, J558, HNK-1, P388D1, P3X63Ag8.653, EL4, and LMTK$^-$ were from the American Type Culture Collection.

WEHI231, S194, MPC-11, J558, P388D1, and LMTK$^-$ were grown in Dulbecco's modified Eagle's medium supplemented with 2 mM glutamine, 50 μg of gentamicin sulfate per ml, and heat-inactivated serum (GIBCO-BRL) that was 10% (S194) or 20% (MPC11) horse serum or 10% fetal calf serum (WEHI231, J558, P388D1, and LMTK$^-$). WEHI231 medium also contained 50 μM 2-mercaptoethanol. The other cell lines were grown in the same basic type of medium with minor modifications. 300-19P, 300-19P-S20, P4-11, P-8, 38B9, 18-81Y, BALB1427, BCL1, and EL4 were grown in RPMI 1640 medium supplemented with 10% heat-inactivated fetal calf serum and 50 μM 2-mercaptoethanol. 300-19P-S20 is a subclone derived in this laboratory from parental line 300-19P by limiting dilution. This subclone was chosen on the basis of the homogeneity of its unrearranged kappa gene. P4-11 and P-8 are Dμ- and μ-expressing progeny, respectively, of 300-19P (62). 26-4 BAMC1, BASC6C2, and HAFTL1 were grown in RPMI 1640 with 15% heat-inactivated fetal calf serum and 50 μM 2-mercaptoethanol. LyD9 was maintained in RPMI 1640 with 10% WEHI-3 conditioned medium and 10% heat-inactivated fetal calf serum, 50 μM 2-mercaptoethanol, and 50 μg of gentamicin per ml.

The pro- and pre-B-cell lines used in this study were extensively characterized for possible signs of differentiation or heterogeneity. Fluorescence-activated cell sorter analysis of all pro-B-cell lines showed the same B220 staining pattern as that originally reported (30) and failed to reveal any surface IgM. The kappa gene was verified to be unrearranged in all pro- and pre-B-cell lines, while the heavy-chain gene retained the same rearrangement state as that originally reported (Table 1 contains the relevant references). The parental BASC6C2 and HAFTL1 lines were at least 95% homogeneous at the IgH locus, while the pre-B-cell lines were >99% homogeneous. The HAFTL1 line was similar to foundation line HAFTL1-A in its IgH gene configuration, where both alleles are rearranged (19). Subclones derived from pro-B-cell lines BASC6C2 and HAFTL1 by limiting dilution displayed chromatin patterns and in vivo footprints identical to those of the parental line (data not shown). Northern (RNA) blots showed no detectable kappa mRNA for all pro- and pre-B-cell lines, even after prolonged exposure (Table 1).

DNase I digestion of isolated nuclei. Nuclei were isolated and treated with DNase I as detailed previously (11).

DNase I digestion of permeabilized cells. Cells were permeabilized with lysolecithin on the basis of a procedure published previously (54). The same protocol

was used for all cell lines except LyD9 and WEHI231, for which slight modifications were necessary. Unless otherwise indicated, all manipulations were conducted at room temperature. A total of 7.5×10^7 cells were harvested per cell line. The cells were centrifuged at $1,000 \times g$ for 10 min and resuspended at a concentration of 1.5×10^7/0.4 ml in a permeabilization solution (preequilibrated to 37°C) containing 0.05% lysolecithin (Sigma) in solution I [150 mM sucrose, 80 mM KCl, 35 mM *N*-2-hydroxyethylpiperazine-*N*′-2-ethanesulfonic acid (HEPES) at pH 7.4, 5 mM K_2HPO_4, 5 mM $MgCl_2$, 0.5 mM $CaCl_2$, 0.02% sodium azide (as a preservative)]. The resulting suspension was incubated at 37°C for 1 min. Permeabilization of LyD9 was carried out with a fourfold lower concentration of lysolecithin (0.0125%) to prevent aggregation. For WEHI231, all solutions included 1.0 mM ethylene glycol-bis(β-aminoethyl ether)-*N*,*N*,*N*′,*N*′-tetraacetic acid (EGTA) to prevent endogenous nuclease activity during the various manipulations. After permeabilization, the cells were spun at $1,000 \times g$, washed with solution I, distributed to microcentrifuge tubes at 1.5×10^7 cells per tube, and recentrifuged.

Each tube of 1.5×10^7 cells was resuspended in 400 μl of solution II (150 mM sucrose, 80 mM KCl, 35 mM HEPES at pH 7.4, 5 mM K_2HPO_4, 5 mM $MgCl_2$, 1 mM $CaCl_2$, 0.02% sodium azide) and treated with an appropriate concentration of DNase I (Worthington Biochemicals) at room temperature for 5 min. The reaction was stopped by spinning the mixture in an Eppendorf microcentrifuge at 1,500 rpm for 10 min, removing the supernatant, and resuspending the DNase I-treated cells in 200 μl of stop solution (20 mM Tris-HCl at pH 8.0, 20 mM NaCl, 20 mM EDTA, 1% sodium dodecyl sulfate [SDS], 600 μg of proteinase K per ml), which was incubated at 37°C from 3 h to overnight. Afterwards, the lysate was diluted with 200 μl of a solution containing 150 mM NaCl and 5 mM EDTA. The samples were extracted sequentially with phenol-chloroform (1:1) and chloroform-isoamyl alcohol (24:1) and then ethanol precipitated. RNA was removed by treatment of the DNA pellet with 100 μg of RNase A per ml at 37°C for 2 h, followed by digestion with 200 μg of proteinase K per ml at 37°C for 2 h and another round of phenol-chloroform extraction and ethanol precipitation. The DNA pellet was recovered, washed in 80% ethanol, dried, resuspended in 200 μl of TE (10 mM Tris at pH 8.0, 1.0 mM EDTA), and quantitated with a Hoefer DNA fluorometer.

MNase digestion of permeabilized cells. Cells were permeabilized, washed, and distributed to microcentrifuge tubes as described for the DNase I protocol. Each tube of 1.5×10^7 cells was treated with 0, 10, 20, 30, or 40 U of MNase per ml (Worthington Biochemicals) at room temperature for 5 min in MNase buffer (150 mM sucrose, 50 mM Tris-HCl at pH 7.5, 50 mM NaCl, 2.0 mM $CaCl_2$, 0.02% sodium azide) instead of solution II. The reaction was stopped, and DNA was isolated as described for the DNase I protocol. For the DNA controls, naked genomic DNA (200 μg/ml) was digested with 0, 1, 2, 4, or 8 U of MNase I per ml at room temperature for 5 min. The reaction was stopped, and the DNA was purified as described above.

Indirect end-labeling analysis. Nuclease digests were restricted with *Bgl*II and analyzed on a 1.4% agarose gel in 1× TAE (40 mM Tris-acetate, 1 mM EDTA). Samples were electrophoresed at 1 V/cm for 24 h. The DNA was blotted onto a Bio-Rad Zeta Probe nylon membrane by a modified alkaline blotting protocol (61). The gel was blotted overnight in 0.4 M NaOH-0.2 M NaCl. The membrane was then neutralized in 50 mM Tris at pH 7.5 for 5 to 10 min, air dried, and baked at 80°C under a vacuum for 1 h. Prehybridization was carried out from 2 h to overnight in 0.27 M NaCl–15 mM sodium phosphate (pH 7.0)–1.5 mM EDTA–0.5% BLOTTO dried milk powder–1% SDS–500 μg of sonicated herring testis DNA per ml. Hybridization was carried out overnight in the same buffer in the presence of at least 2.5×10^7 cpm of a radiolabeled DNA probe (specific activity, at least 10^9 cpm/μg) generated by random-primer synthesis with a Decaprime DNA labeling kit (Ambion, Austin, Tex.). The DNA probe used was a 300-bp *Xba*I-*Eco*RI restriction fragment of the kappa locus found just downstream of E3′. After overnight hybridization, membranes were rinsed briefly for 5 min and then for 15 min at room temperature with 0.5× SSC (1× SSC is 0.15 M NaCl plus 0.015 M sodium citrate)–20 mM sodium phosphate (pH 7.0)–2% SDS and then four times for 20 min each time at 65°C in 0.1× SSC–20 mM sodium phosphate (pH 7.0)–2% SDS. Blots were air dried briefly and exposed to Kodak XAR-5 film with an intensifying screen at −80°C for 4 to 10 days. Autoradiograms were calibrated with DNA standards 2.3, 2.0, 1.3, 1.1, and 0.87 kb long by constructing a plot of log DNA size versus mobility. The sizes of the resulting hypersensitive fragments were interpolated from the resulting linear fit.

RNA isolation and Northern blot analysis. Total cellular RNA was isolated from various cell lines and analyzed on Northern blots by hybridization with a ^{32}P-radiolabeled Cκ-specific or human actin probe as previously described (12). Processed blots were exposed to X-ray film with an intensifying screen at −80°C, and RNA levels were quantitated by densitometric scanning of autoradiographic films (12). Kappa mRNA levels in the various cell lines were compared after normalization with respect to actin RNA (Table 1).

In vivo footprinting. Cells were treated with dimethyl sulfate (DMS) in vivo by a modified form of a previously published procedure (55). Briefly, 5×10^7 cells were resuspended in 2.0 ml of medium and treated with 0.1% DMS for 10 min at room temperature. The reaction was quenched by 10-fold dilution with ice-cold 1× PBS (0.137 M NaCl, 2.6 mM KCl, 10 mM Na_2HPO_4, 1.8 mM KH_2PO_4, pH 7.4) and centrifugation at $1,500 \times g$ for 10 min at 4°C. The cellular pellet was washed twice with a 10-fold volume of ice-cold PBS and lysed in 1.5 ml of harvest buffer containing 20 mM Tris-HCl at pH 8.0, 20 mM NaCl, 20 mM EDTA, 0.1% SDS, and 300 μg of proteinase K per ml at 37°C from 5 h to overnight. The methylated DNA sample was phenol-chloroform extracted, ethanol precipitated twice, dried, and cleaved in 200 μl of 1.0 M piperidine at 95°C for 30 min. Piperidine was removed by repeated lyophilization in a Speedvac concentrator; each time, the DNA pellet was resuspended in 500 μl of water between freeze-drying cycles. This step was done three times. The cleaved DNA was quantified by fluorimetry with Hoechst dye, and an aliquot was analyzed on a 1.5% agarose gel. This treatment typically yielded an average fragment length of about 500 bp.

In vitro methylation of genomic DNA. Genomic DNA was isolated as described previously (11). DNA was methylated by treating 200 μl of a 1-mg/ml genomic DNA solution with 5 μl of a 20% DMS solution (prepared in ethanol), followed by incubation at room temperature for 30 s. The reaction was quenched by adding 50 μl of ice-cold stop buffer (1.5 M sodium acetate, 1.0 M 2-mercaptoethanol, 100 μg of yeast tRNA per ml) and 750 μl of 100% ethanol chilled to −20°C. The DNA was pelleted, washed with 75% ethanol, dried, and resuspended in 200 μl of 1.0 M piperidine. The methylated DNA sample was cleaved by incubation at 95°C for 30 min. Piperidine was removed by repeated lyophilization as described for the in vivo samples. The cleaved DNA was quantified and analyzed on an agarose gel as described above.

Primers. The following primers were used for each sequential step in the LMPCR protocol (44): primer A for first-strand synthesis, primers B and B′ for PCR amplification, and radiolabeled primer C for the last primer extension step. To footprint the core region's lower strand, the primer set of oligonucleotides (oligos) 8, 3, and 31 were used as primers A, B, and C, respectively. On occasion, oligo 11 was used instead of oligo 31 as primer C. The core region's upper strand was footprinted by using oligos 18, 17, and 30 as primers A, B, and C, respectively. Oligo 7B replaced oligo 30 in certain cases. The sequences of these oligos are as follows: 8, CATACCAGACTGGTTATTGA; 3, ATGGTGACTGGCCT GAGAAG; 31, GGTGACTGGCCTGAGAAGATTA; 11, GCACTCCACACC CTTTCAAG; 18, GTGCAAAAGCATTGGGACTG; 17, CTGGGGACTAAC CTGGGGCT; 30, GGGGACTAACCTGGGGCTTGAG; 7B, GGATGGGAG CGAAAGCAACAGATGT. The ligation linker sequence was derived from Mueller and Wold (44) and consisted of oligo 32 (GCGGTGACCCGGGAGA TCTGAATTC) and a shorter complementary strand, oligo 33 (GAATTCAGA TC). Oligo 32 also served as primer B′ for the PCR. To footprint the HSS1-HSS2 bottom-strand region, oligos 45 (GCAGTAAGGATCTAAGTGT), 44 (CTAT TGATCTCTGCAACAACAG), and 43 (CTGCAACAACAGAGAGTGTTA GA) were used as primers A, B, and C, respectively.

LMPCR. DMS-treated and piperidine-cleaved DNA samples were subjected to LMPCR as described previously (44). For first-strand synthesis, 5 μg of DNA was combined with 0.3 pmol of primer A and 3 μl of 5× Mg-free Sequenase buffer (200 mM Tris at pH 7.7, 250 mM NaCl) in a final volume of 15 μl. The DNA was denatured at 95°C for 3 min and annealed at 60°C for 30 min. The tubes were then quick spun at 4°C and placed on ice. A 7.5-μl volume of an Mg-dithiothreitol (DTT)-deoxynucleoside triphosphate mixture (20 mM $MgCl_2$, 20 mM DTT, 0.2 mM deoxynucleoside triphosphate mixture [Pharmacia]) was then added, followed by 1.5 μl of Sequenase version 2 (United States Biochemical [USB]) diluted 1:4 with TE. This reaction mixture was incubated at 43°C for 5 min. The enzyme was subsequently heat inactivated at 60°C for 5 min; this was followed by addition of 6 μl of 310 mM Tris-HCl and further incubation at 67°C for 10 min. The reaction mixture was then quick spun and placed on ice.

The oligo linker (oligos 32 and 33) was ligated to the Sequenase-repaired DNA samples by addition of 20 μl of ligase dilution solution (17.5 mM $MgCl_2$, 42.3 mM DTT, 125 μg of bovine serum albumin [BSA] [nuclease free, from Promega] per ml) and 25 μl of the ligase mixture (10 mM $MgCl_2$, 20 mM DTT, 3 mM ATP [Pharmacia], 50 μg of nuclease-free BSA per ml, 50 mM Tris at pH 7.7, 4 μM unidirectional linker [oligos 32 and 33 annealed together], 3 U of T4 DNA ligase [Promega]). Ligation proceeded at 18°C for 17 to 20 h. The ligase was heat inactivated at 70°C for 10 min and DNA was precipitated at −20°C for 2 h after the addition of 9.4 μl of a precipitation salt mixture (2.7 M sodium acetate, 1.0 mg of yeast tRNA per ml) and 220 μl of 100% chilled ethanol. The DNA pellet was collected by centrifugation, washed with 500 μl of 75% ethanol chilled to −20°C, dried, and resuspended in 70 μl of distilled water. To PCR amplify the ligated DNA sample, 25 μl of a *Taq* salt mixture (150 mM NaCl, 38 mM Tris [pH 8.0]), 12.5 mM $MgCl_2$, 10 pmol of primer B, 10 pmol of primer B′, 20 nmol of each deoxynucleoside triphosphate) and 5 μl of diluted *Taq* polymerase (1 U/μl) were added. Eighteen rounds of PCR were carried out with the following cycling profile: the first denaturation was done at 94°C for 5 min, and all subsequent denaturation was done for 1 minute at 94°C. The annealing step was done at 63°C for 2 min. All extensions were conducted at 76°C for 3 min, except the final extension, which took 10 min. The samples were then placed on ice.

Following PCR amplification, the final primer extension (labeling step) was performed by addition of 10 μl of a label mixture (1× *Taq* buffer, 3 pmol of ^{32}P-labeled primer C [1×10^6 to 3×10^6 cpm/pmol], 10 to 20 nmol of a deoxynucleoside triphosphate, 3 to 3.5 U of *Taq* DNA polymerase) and followed by denaturation at 94°C for 5 min, annealing at 65°C for 2 min, and extension at 76°C for 10 min. The reaction was terminated by addition of 295 μl of *Taq* Stop Solution (260 mM sodium acetate, 10 mM Tris, 4 mM EDTA at pH 8.0, 35 μg of yeast tRNA [Sigma] per ml). The sample was phenol-chloroform extracted, ethanol precipitated, washed, and dried. The dried pellets were counted in a scintillation counter and resuspended in 8 μl of formamide dye (USB). Equal

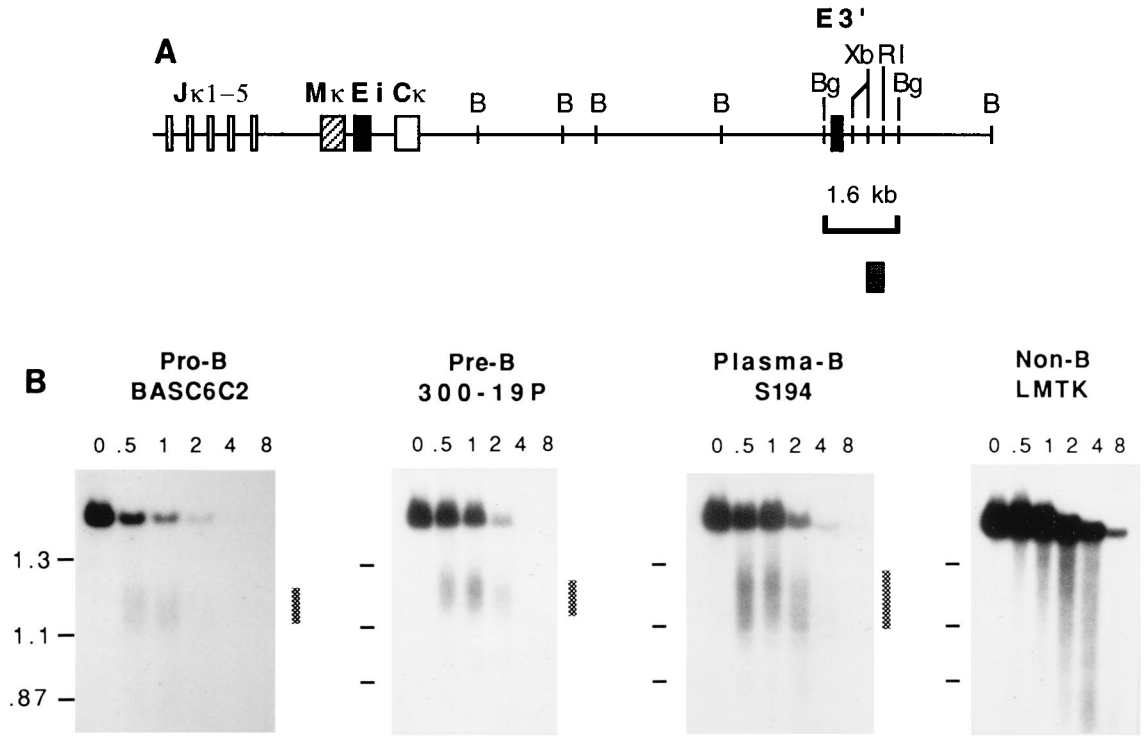

FIG. 1. (A) Strategy for indirect end labeling. The restriction map of the immunoglobulin κ locus in its germ line state shows the Jκ1-5 (joining) and Cκ (constant) exons as open boxes. Filled boxes represent the intronic enhancer (Ei) and E3′; the diagonally striped box is the kappa matrix attachment region (Mκ). Bg, B, Xb, and RI are restriction sites for *Bgl*II, *Bam*HI, *Xba*I, and *Eco*RI, respectively. The reference *Bgl*II restriction fragment is 1.6 kb long. DNase I-hypersensitive sites within this region were mapped with respect to the *Bgl*II site downstream by using an *Xba*I-*Eco*RI restriction fragment as a hybridization probe (checkered box). (B) DNase I-hypersensitive site analysis of E3′ in nuclei isolated from different B-cell lines. Nuclei were isolated from the indicated cell lines and digested with increasing concentrations of DNase I from 0 to 8 μg/ml. The DNA was purified, cut with *Bgl*II, and analyzed on a Southern blot by using the probe shown in panel A. Markers to the left of each gel are molecular size standards (1.3, 1.1, and 0.87 kb). The checkered box to the right marks the hypersensitive region.

counts of 200,000 to 700,000 cpm were loaded per lane on a 6% denaturing polyacrylamide gel. Gels were dried and exposed to FUJI film with an intensifying screen at −80°C for 6 h to 1 week. To localize the G residues on the enhancer sequence, a sequencing reaction of a subcloned enhancer fragment was run alongside the LMPCR samples by using the appropriate LMPCR primer C in the Sanger dideoxy sequencing reaction. The dideoxy-C reaction was specifically informative in identifying the footprinted G residues. To determine whether a site was partially or completely protected, the autoradiographic bands were scanned with a Molecular Dynamics laser densitometer and normalized to reference bands showing equal intensity across the various samples. The ratio obtained was compared with that of the naked DNA or non-B-cell controls. Band intensities reduced to less than 40% of controls were judged to be completely protected, while those reduced to values greater than 40% of controls were partially protected.

Nuclear extract preparation and mobility shift assay. Nuclear extracts were prepared as described by Dignam et al. (20). All solutions contained DTT (0.5 mM) and the protease inhibitors aprotinin (1 μg/ml), leupeptin (1 μg/ml), and phenylmethylsulfonyl fluoride (0.5 mM). Protein concentrations were measured with the Bradford assay (13). Oligos for mobility shift assays, namely, DP and H2A2.2, were end labeled with [α-^{32}P]dATP and [α-^{32}P]dCTP (>3,000 Ci/mmol; ICN) by using the large Klenow fragment of DNA polymerase (Promega) or [γ-^{32}P]ATP (>4,500 Ci/mmol; ICN) by using T4 polynucleotide kinase (USB). The binding reactions were carried out in a total volume of 30 μl containing 50,000 cpm of the labeled probe, 1 μg of poly(dI-dC) (Pharmacia), 12 μg of nuclear extract, 10 mM Tris-HCl (pH 7.5), 1 mM EDTA, 1 mM β-mercaptoethanol, 4% glycerol, and 80 mM KCl. The reaction mixtures were incubated for 30 min at room temperature and loaded onto a 5% polyacrylamide gel (acrylamide-bisacrylamide ratio, 19:1) made up in running buffer containing 50 mM Tris, 0.38 M glycine, and 2 mM EDTA. The samples were subjected to electrophoresis at 8 V/cm. The gel was dried and exposed to FUJI film with an intensifying screen overnight at −80°C. Competition experiments were performed under the same binding conditions by using a 100-fold excess of competitor. The sequences of double-stranded oligos are as follows (the numbers indicate the relevant nucleotide positions of κE3′, and the lowercase letters represent overhangs): DP, 413 to 438, taccCTTGATCAAAGCAGTGTGACGG TAGC; DP-m1, gaccCTTGATCAAAGCAGTATGATGGTAGC; DP-m2, gac cCTTAATTAAAGCAGTGTGACGGTAGC; H2A2.2, GTGACGCAGCGGT GGGTGACGACTG; PU.1, 445 to 469, CTTTGAGGAACTGAAAACAG AACCT; E-BOX, 555 to 584, TACACCTGCTCCCTACCCCAGCACCTGG CC.

RESULTS

E3′ becomes DNase I hypersensitive prior to kappa gene rearrangement. To determine at what point during B-cell differentiation E3′ first becomes activated, we probed its chromatin structure with DNase I in B-cell lines arrested at various points of development. The cell lines used in this study are listed in Table 1, and the organization and expression of their immunoglobulin genes are indicated. In the initial phase of our investigation, E3′ chromatin was studied in nuclei isolated from pro-B cells (BASC6C2), pre-B cells (300-19P-S20), plasma cells (S194), and non-B cells (LMTK$^-$). Figure 1A displays a restriction map of the immunoglobulin κ locus and the indirect end-labeling strategy (75) used for mapping of hypersensitive sites at κE3′. Preferred sites of DNase I cleavage were mapped with respect to a *Bgl*II site downstream by using a proximal *Xba*I-*Eco*RI fragment (checkered box) as the hybridization probe. The result of this analysis is shown on a Southern blot in Fig. 1B. While untreated nuclei (lane 0) yielded a 1.6-kb *Bgl*II restriction fragment, DNase I digestion (lanes marked with concentrations of 0.5 to 8 μg/ml) resulted in the appearance of specific subbands 1,150 to 1,300 bp long. These subbands mapped to E3′ and were observed only in B lineage cells (BASC6C2, 300-19PS20, and S194 but not fibroblast line LMTK$^-$). We verified that preferential cutting at these sites is

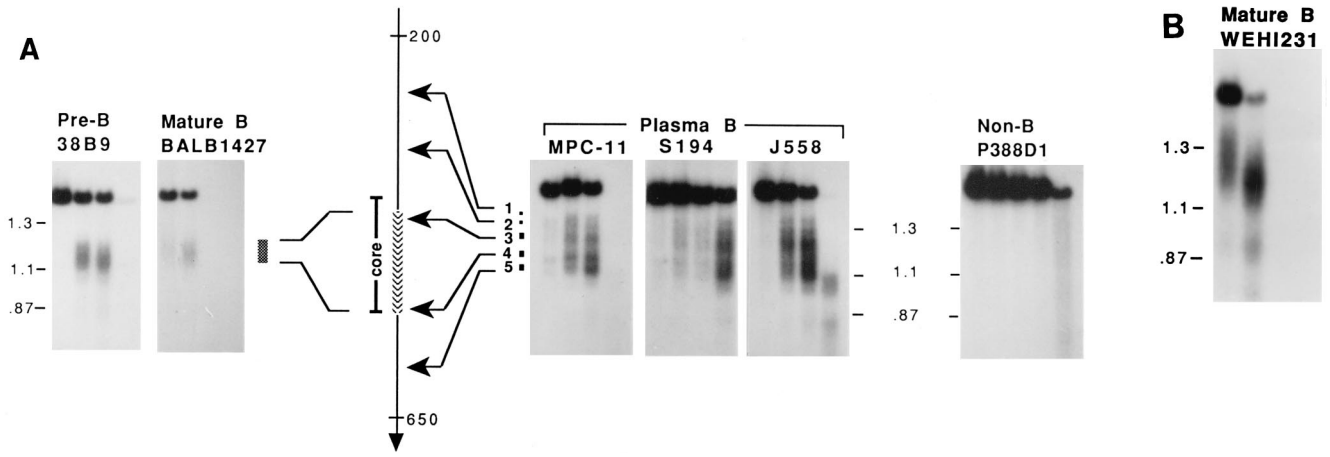

FIG. 2. DNase I-hypersensitive site analysis of E3′ in permeabilized cells. Cells were permeabilized with lysolecithin and incubated with 0, 0.5, 1.0, or 2.0 μg of DNase I per ml (from left to right within each panel), except for P388D1 cells, which received 4.0 μg of DNase I per ml. In panel B (see Materials and Methods for special conditions used for WEHI231 cells), four DNase I concentrations are shown: 2.0, 4.0, and 8.0, and 16.0 μg/ml. After enzyme treatment, DNA was purified, cut with *Bgl*II, and analyzed on a Southern blot as for Fig. 1B. The hypersensitivity pattern shown here in 38B9, BALB1427, and WEHI231 cells is referred to in the text as the type E chromatin structure, while that found in MPC11, S194, and J558 cells is referred to as the type L structure. A vertical plot of E3′ with nucleotide positions 200 and 650 indicated for orientation is shown with the transcriptional core region marked. The checkered box to the right of the BALB1427 gel depicts the type E hypersensitive region. The numbered dots to the left of the MPC11 gel indicate the positions of five type L HSSs: HSS1 to HSS5. Markers of 1.3, 1.1, and 0.87 kb are shown as molecular size standards. Hypersensitive positions within the E3′ sequence were mapped by subtracting the hypersensitive fragment size from the parental *Bgl*II restriction fragment (1,590 ± 30 bp) and then adding 80 bp to account for the position of the 5′ *Bgl*II site within the enhancer. Hypersensitive fragment sizes were determined as described in Materials and Methods. For type E, fragments typically measured 1,150 to 1,270 bp. For type L, average lengths of HSS1 to HSS5 were 1,400, 1,330, 1,250, 1,150, and 1,080 bp, respectively.

a unique property of chromatin since limit digestion of naked genomic DNA showed only random cuts (data not shown). These observations are consistent with the tissue-specific nature of E3′ transcriptional function and support findings in our previously published work (11). Interestingly, the E3′ region was found to be hypersensitive not only in plasmacytoma S194 cells, where the kappa gene is actively transcribed, but also in pro-B-cell line BASC6C2 and pre-B-cell subclone 300-19P-S20 (Fig. 1B). Nuclease accessibility in BASC6C2 and 300-19P-S20 cells was limited to a 120-bp region which coincided with the core region of the enhancer. Hypersensitivity in plasmacytoma S194 cells, on the other hand, encompassed a larger area (see further experiments below). Since we verified the kappa gene in both BASC6C2 and 300-19P-S20 cells to be unrearranged by Southern blot analysis (data not shown), these results indicate that E3′ assumes an open chromatin configuration prior to kappa gene rearrangement.

Rapid permeabilization technique reveals two types of DNase I-hypersensitive patterns at E3′. To verify the generality of our findings, we surveyed an additional number of independently derived transformed cell lines. To circumvent the lengthy nuclear isolation protocol, we adapted a rapid method that makes use of lysolecithin to permeabilize cells to DNase I (54). It has been shown that treatment of cells with this phospholipid does not perturb transcription and replication processes, thus maintaining the structure of chromatin (16, 78). Compared with our nuclear isolation protocol, the lysolecithin method was quick, yielded precisely the same hypersensitive pattern, and caused less perturbation of DNA-protein interactions. Moreover, since losses were minimized, fewer cells were required for the experiment. Representative results are shown in Fig. 2. Consistent with data obtained with isolated nuclei, we observed hypersensitive sites only in cells of the B lineage (38B9, BALB1427, WEHI231, MPC-11, S194, and J558 but not P388D1). Two patterns of DNase I hypersensitivity were observed. The first pattern, which we designated type E (for early), was observed in pro-B-cell, pre-B-cell, and mature B-cell lines, as exemplified by 38B9, BALB1427, and WEHI231 in Fig. 2. In this structure, the accessible site was spread over 120 bp which we mapped to the E3′ core region (nucleotide positions 400 ± 30 to 520 ± 30 of κE3′ [numbering system according to reference 41]). The early mature B-cell line BALB1427 exhibited the type E pattern, although the more advanced mature B-cell line WEHI231 tended to show a modified form of hypersensitivity which extended upstream of the core region at early points of digestion (Fig. 2B). This accessible region disappeared quickly at higher enzyme concentrations, being reduced to the type E form. A dramatically different hypersensitive structure was observed in plasmacytoma lines MPC-11, S194, and J558 (Fig. 2). The new pattern, which we designated type L (for late), is characterized by a wider area of hypersensitivity, confirming initial observations with isolated S194 nuclei (Fig. 1B). The expanded region, which covered 320 bp, extended upstream to nucleotide 270 ± 30 and downstream to nucleotide 590 ± 30. Five reproducible hypersensitive subbands (HSS) were discerned, and they are labeled 1 to 5 in Fig. 2A. We also noted faint subbands that appeared below the major hypersensitive bands only at high DNase I concentrations (bands migrating close to the 1.1- and 0.87-kb markers in lane 2 of WEHI231 and lane 4 of J558). These subbands could represent cleavages at the linker regions of nucleosomes and are addressed further in Fig. 10.

A summary of all of the cell lines surveyed is presented in Table 1. The type E pattern was consistently found in all pro-B-cell, pre-B-cell, and mature B-cell lines, with the exception of early progenitor B-cell line LyD9, in which no hypersensitive structure was detected (Table 1). Surprisingly, λ light-chain producers exhibited hypersensitive sites at κE3′ as well. BCL1, a mature B-cell line, exhibited the type E structure, while J558, a plasmacytoma-derived line, showed the type L structure. Northern blot analysis of these λ producers revealed the presence of stable kappa transcripts, indicating that the kappa locus is still transcriptionally active, despite the lack of a functional kappa polypeptide (Table 1). The chromatin pat-

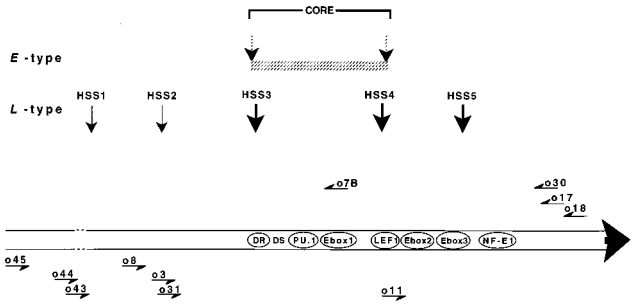

FIG. 3. Strategy for LMPCR in vivo footprinting. The two types of DNase I-hypersensitive patterns (E and L) are represented schematically and mapped with respect to the E3′ diagram below (long horizontal arrow). Type E hypersensitivity is represented by a horizontal hatched bar whose boundaries are demarcated by vertical arrows. Type L HSSs are depicted by vertical arrows labeled HSS1 to HSS5. E3′ is drawn pointing in the 5′-to-3′ transcriptional direction of the kappa gene. The break (broken line) in the continuity of the sequence indicates that the distance between the two sides is not drawn to scale. Approximate locations of factor-binding sites are indicated, and encircled sites indicate that DNA-binding activity was identified in vitro. Short half arrows represent the oligo primers used for LMPCR. Each oligo is named with the letter o followed by a number.

terns thus reflect those found in κ-producing cell lines at the same developmental stage (Table 1). IgM-secreting hybridoma line HNK-1 and its nonsecreting parental myeloma line P3X63Ag8.653 exhibited the type L structure characteristic of other plasmacytoma lines. On the basis of our Northern blot analysis, the plasmacytomas surveyed expressed 5- to 300-fold higher levels of κ mRNA than the mature B-cell lines (Table 1). Thus, while the type E pattern of DNase hypersensitivity was consistently observed in pro-B cells, pre-B cells, and mature B cells, the type L pattern predominated in plasma stage cells. The shift from type E to type L chromatin therefore correlates with increased kappa mRNA expression and the differentiation state of the B cell.

Core region footprints correlate with type E chromatin. DNase I-hypersensitive sites coincide with nucleosome-free regions in chromatin typically caused by the binding of regulatory protein factors to specific sites (25). To determine the nucleotide residues involved in the formation of type E and type L chromatin, we utilized DMS as a probe in the LMPCR footprinting protocol (44). Although previous in vivo footprinting analysis of κE3′ detected DMS protection at the DR-DS region, the PU.1–NF-EM5 site, and the E box 1 motif in two mature human B-cell lines (Fig. 3) (31), neither early cells (pro- or pre-B cells) nor plasmacytoma lines were investigated in that study. Thus, those results do not adequately explain the changing chromatin patterns that we observed in murine cell lines. By using our DNase I-hypersensitive site maps as a guide, we designed oligo primers to analyze various regions of E3′ (Fig. 3). The primer set of oligos 8, 3, and 31 was utilized to footprint the core and downstream regions of the lower strand, while the primer set of oligos 18, 17, and 30 was employed to analyze the complementary upper strand. Finally, primers 45, 44, and 43 were utilized to analyze regions upstream of the core region. The in vivo footprinting results are shown in Fig. 4, 6, 7, and 8 and summarized on a diagram of the κE3′ sequence in Fig. 5.

Figure 4 shows the results of two LMPCR experiments which analyzed the lower-strand interactions. The non-B-cell control EL4 (lane 14) exhibited the same methylation pattern as naked DNA (lanes 1, 7, 8, and 15), confirming that histones do not interfere with DMS methylation (38). Thus, any observed differences between the various B-cell lines and the control must result from the binding of a cell-specific factor. Focusing on the core region of the enhancer, we first noted a B-cell-specific hypersensitive G at position 402 (filled circle in Fig. 4, lanes 9 to 13). This was followed by footprints at G405, G409, G414, G417, G418, and G421 which encompass the DR region (open and slashed circles indicate complete and partial protection, respectively). The relatively low reactivity to DMS of G residues within this region as observed even in naked DNA (lanes 8 and 15) made it difficult to judge the presence of footprints at certain sites. However, the marked B-cell-specific protections were reproducible. For the upper strand, partial protection at G-407 was detected in mature and plasma cells (Fig. 6, lanes 3 to 5). The G-409 to 421 footprints were present at all stages of development, with the strongest footprint found in mature B-cell line WEHI231 and plasmacytoma line J558 (Fig. 4). These results are summarized in Fig. 5A.

The most striking developmental change was observed at the junction of the DR and DS regions (Fig. 4 and 6). Specific protection of G-423 and G-435 in the lower strand was observed at the pro-B-cell (BASC6C2), pre-B-cell (300-19P-S20), and mature B-cell (BALB1427 and WEHI231) stages but not at the plasma cell (S194, MPC11, and J558) stage (Fig. 4, lanes 2 to 6 and 9 to 13). Similarly, on the upper strand, pro-B-cell- and mature B-cell-specific but not plasma cell-specific footprints were observed at G-419 and G-432 (Fig. 6, lanes 2 and 3 but not lanes 4 and 5). These protections were separated by a hypersensitive G at position 427. G-419 and G-423 together form part of a sequence (GTCAC) that exhibits a dyad axis of symmetry (Fig. 5A). Likewise, G-432 and G-435 constitute part of a perfect palindrome (TTGATCAA). The coordinate disappearance of these footprints at the plasma cell stage is most interesting because it correlates with the switch from type E to type L chromatin (Fig. 5A).

The PU.1–NF-EM5 and E box 1 sites were unequivocally occupied throughout development (Fig. 4 and 6). B-cell-specific reactivity at the PU.1–NF-EM5 site was observed as a hypersensitive G at position 455 on the lower strand (Fig. 4, lanes 2 to 6 and 9 to 13) and as protected sites at G-451 and G-452 (PU.1-binding site) and G-457 (NF-EM5-binding site) on the upper strand (Fig. 6, lanes 2 to 5). We further verified the upper-strand footprints by replacing oligo 30 with more proximal oligo 7b as the labeled primer (data not shown). The observed footprints are consistent with methylation interference data characterizing PU.1–NF-EM5 interactions with DNA in vitro (59) and suggest that these factors bind E3′ as early as the pro-B-cell stage. E box 1 (CATCTG) at positions 476 to 481 (Fig. 5) has been shown previously to play an important role in E3′ transcriptional function (31, 57). G-476 on the lower strand (Fig. 4, lanes 2 to 6) and G-481 on the upper strand (Fig. 6, lanes 2 to 5) were partially protected in pro-B cells, becoming more fully protected in mature and plasma B cells. Eight bases downstream on the lower strand, G-489 protection was observed in mature B cells, becoming more clearly footprinted in plasma cells (Fig. 4, compare lanes 3 and 4 with lanes 5 and 6). The factor responsible for this footprint was not identified, although the transcriptional importance of this site has previously been noted (31). Finally, a hypersensitive G was observed at positions 511 and 512 in plasmacytomas J558 and S194 but not in MPC11 (Fig. 4, lanes 5, 6, 12, and 13). These bases lie in the vicinity of HSS4.

Mature and plasma stage-specific protections are observed at E boxes downstream of the core region. The extension of DNase I hypersensitivity to areas outside of the core region in type L chromatin led us to examine the protein-DNA interactions downstream. In vivo evidence for the binding of nuclear factors to this region (HSS4-5) has not been reported, although

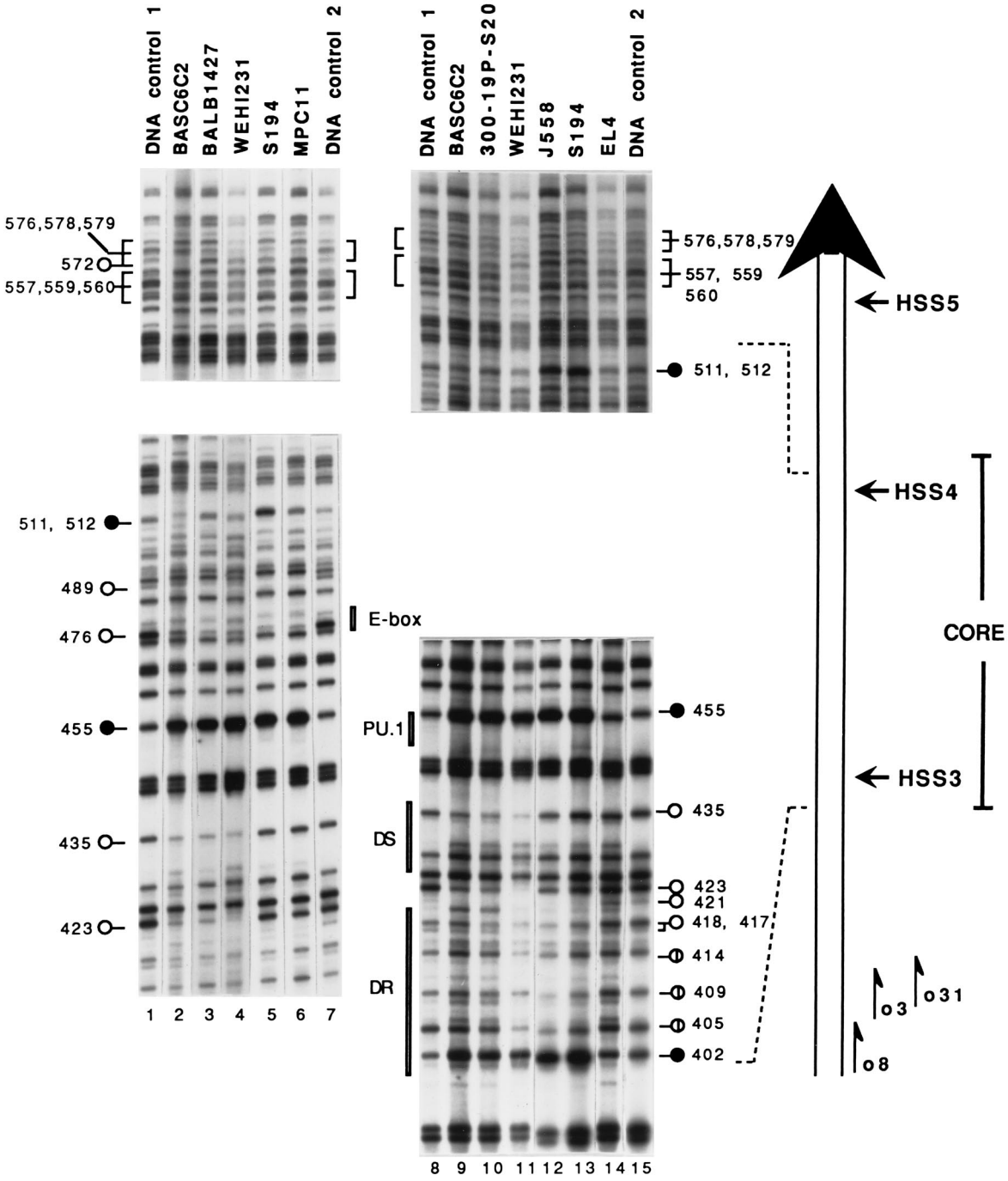

FIG. 4. In vivo methylation pattern in the lower strand of the HSS3-to-HSS5 region. Cultured cells or naked genomic DNAs (DNA controls) were treated with DMS in vivo or in vitro, respectively. The DNA methylation patterns were analyzed by LMPCR by utilizing the primer set of oligos 8, 3, and 31. Lanes 1 to 7 and 8 to 15 represent independent LMPCR experiments. The names of the cultured cell lines are indicated above the lanes, and their descriptions are given in Table 1. The DNA controls were obtained from 38B9 (lane 8) and P388D1 (lane 15) cells. In the course of these experiments, many other different sources of naked genomic DNA controls were used with no differences in the methylation patterns obtained. Open circles denote full guanine (G) protection, filled circles show enhancement, and slashed circles show partial G protection. Beside each symbol is indicated the numbered position of the G residue on the enhancer sequence according to reference 41. The approximate locations of factor-binding sites are marked next to the relevant gel positions. A schematic diagram of the enhancer is shown on the right with the core region, HSSs, and the sites of hybridization of the oligo primers indicated.

LEF-1-like and E12/E47-like factors have been found to bind sequences within this region in vitro (40). Initial evidence of in vivo interactions within this region became apparent in Figure 4. In DNA and non-B-cell controls (lanes 1, 7, 8, 14, and 15), G-557 to 560 and G-576 to 579 (middle G stretches of the bracketed region) were observed to be more susceptible to DMS methylation than the flanking G residues. The pro-B-cell and pre-B-cell lines studied shared this G reactivity (lanes 2, 9, and 10), except for a BASC6C2-specific footprint at G-572 (lane 2). In contrast, mature and plasma cells exhibited a

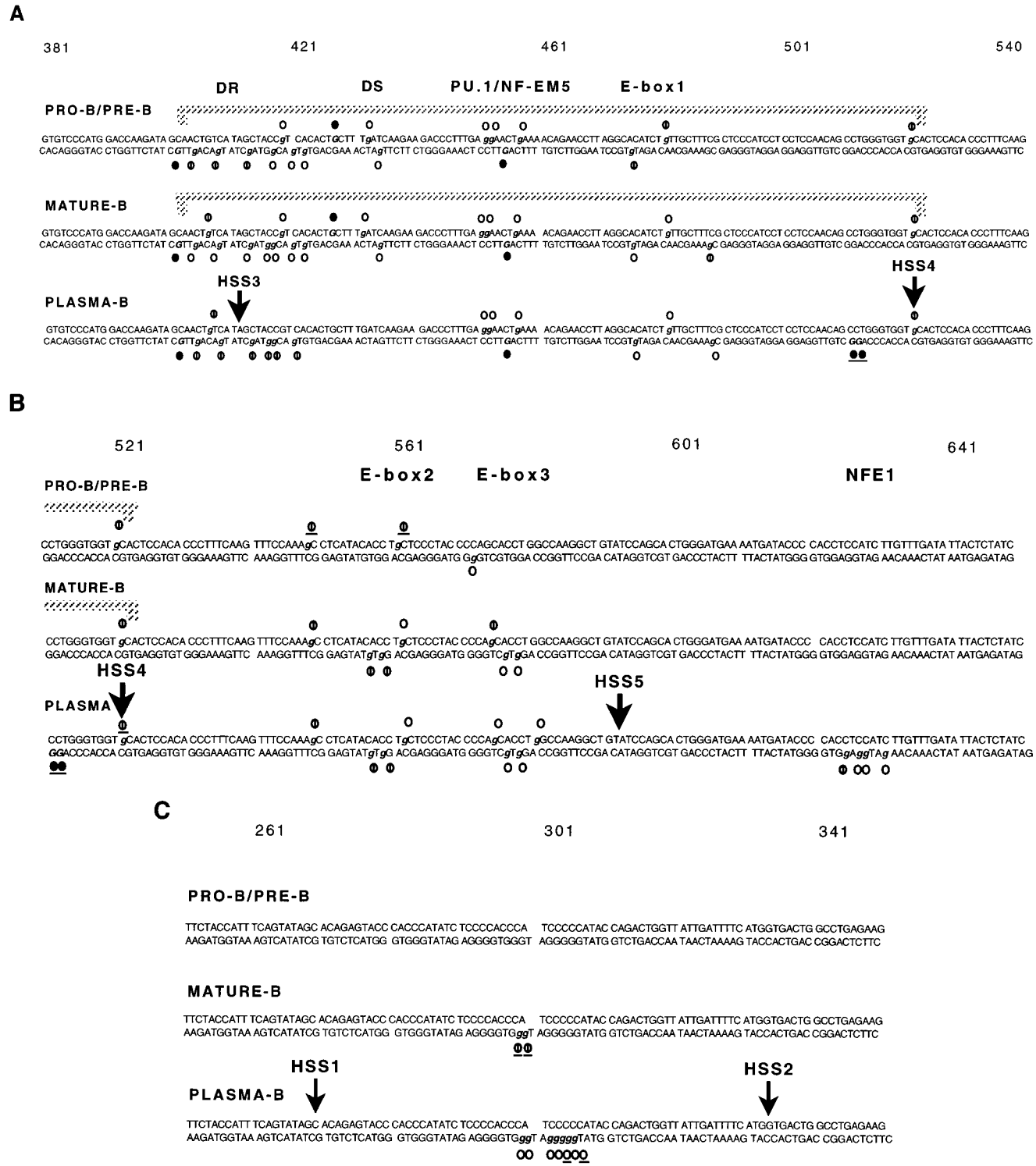

FIG. 5. Summary of results of in vivo footprinting of three regions of mouse κE3′. (A) Core region; (B) downstream region; (C) upstream region. Footprinted G residues are designated *g* and marked with open circles (full protection) or slashed circles (partial protection). Hypersensitive G residues are designated *G* (filled circles). Underlined symbols indicate occurrence in only a subset of the cell lines representing that particular stage. The stippled horizontal bar over the enhancer sequence in panels A and B represents the approximate location of the DNase I-hypersensitive region in type E chromatin. In plasma cells, this structure is replaced by five HSSs (HSS1 to HSS5 of type L chromatin) whose approximate positions (±30 bp) are marked by arrows. Nucleotides are numbered at the top of each panel in accordance with Meyer and Neuberger (41). DR-DS; PU.1; NF-EM5; E boxes 1, 2, and 3; LEF-1; and NF-E1 refer to factor-binding sites (31, 40, 53, 57, 59) as described in the text.

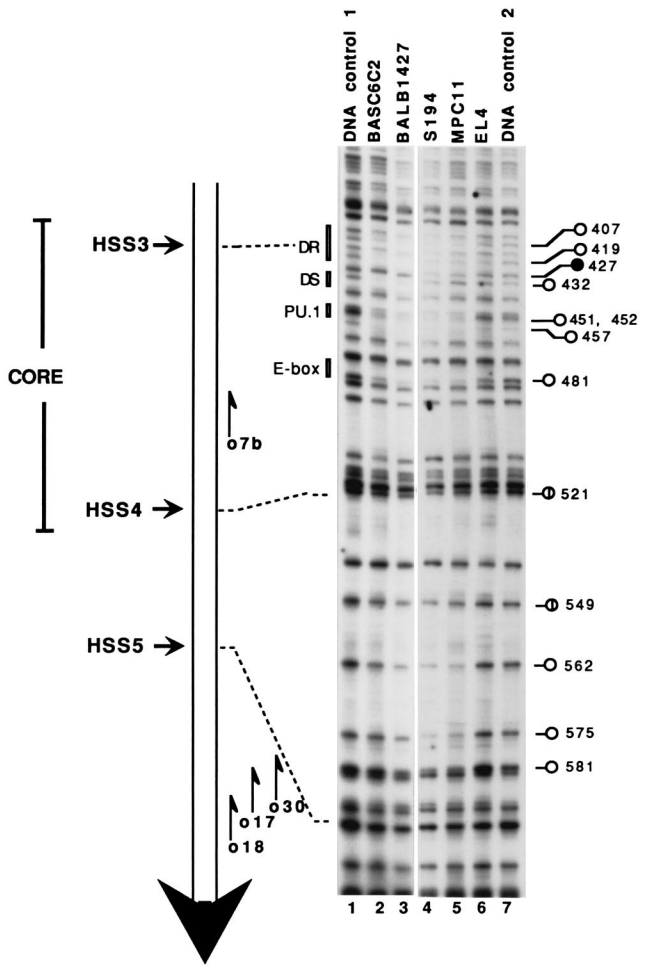

FIG. 6. In vivo methylation pattern in the upper strand of the HSS3-to-HSS5 region. Cultured cells or naked genomic DNAs (DNA controls) were treated with DMS and analyzed by LMPCR utilizing the primer set of oligos 18, 17, and 30. The names of the cultured cell lines are indicated above the lanes, and their descriptions are given in Table 1. DNA control 1 was obtained from 38B9 cells, while DNA control 2 was from P388D1 cells. Open circles denote full guanine (G) protection, filled circles indicate G enhancement, and slashed circles indicate partial G protection. Beside each symbol is the corresponding nucleotide number on the enhancer sequence. The locations of previously characterized factor-binding sites (DR, DS, PU.1, and E box 1) are shown beside the gel. On the left is a schematic diagram of the enhancer showing the core region, HSSs, and the sites of hybridization of the oligo primers.

completely reversed pattern, with the flanking G residues becoming hypersensitive (lanes 3 to 6 and 11 to 13). These results suggested a change in protein-DNA interactions at this site. To define the protected G residues more precisely, we repeated the experiment (Fig. 7A) by utilizing more proximal primer oligo 11 in the labeling step. This analysis verified the results of Fig. 4 and identified partial protection at residues G-557 and G-559 and full protection at G-576 and G-578 in mature B cells and plasma cells but not in pro-B or pre-B cells (lanes 1 to 5). These sites correspond to E boxes 2 and 3. Notably, the BASC6C2-specific footprint at G-572 was again clearly apparent. Interactions on the upper strand were also observed (Fig. 6, bottom). Partial protection was detected at G-521 and G-549, while full protection was observed at G-562, G-575, and G-581 (Fig. 6, lanes 2 to 5). G-562, G-575, and G-581 correspond to E boxes 2 and 3. These results are summarized in Fig. 5B. Although pro-B-cell line BASC6C2 harbored a few partial protections, these did not occur at the E boxes. Strong E-box protection was observed mainly at the mature and plasma B-cell stages, with the extent of occupancy increasing maximally at the plasma B-cell stage (lanes 3 to 5). The results of these analyses demonstrate the binding of factors outside of the core region in vivo.

Plasma-specific footprints at the NF-E1 site and a novel G-C-rich region correlate with type L chromatin. Interactions that occur within the marked HSS4-5 region in Fig. 5B appear insufficient to induce the transition in chromatin structure from E to L. This assertion is based upon the observation that despite the presence of these footprints, mature B cells still exhibit a predominantly type E structure (Fig. 2). Because of the error bars inherent in the mapping of our HSS (±30 bp), we investigated whether any other sequences downstream are footprinted (Fig. 7B). This analysis encompassed nucleotides 623 to 630, the binding site of the putative repressor NF-E1 in early B cells (53). Our results, shown in Fig. 7B, revealed no footprints within this region for early B-cell lines 300-19P-S20 and BASC6C2 and mature B-cell lines BALB1427 and WEHI231 (Fig. 7B, lanes 2, 3, 4, and 5). Surprisingly, protection of NF-E1 sites G-624, G-626, G-627, and G-630 was observed in plasma stage cells (J558 and MPC-11 in lanes 6 and 7). Similar NF-E1-like protections were observed in S194 cells (data not shown). Because these footprints resemble the NF-E1 interactions with its binding site (53) and since no other consistent protections were detected within at least 130 bp downstream of this site, we conclude that the binding of an NF-E1-like factor is involved in the formation of HSS4 and HSS5 in type L chromatin. Contrary to expectations, we did not detect NF-E1 footprints in early B-cell lines.

To investigate the formation of HSS1 and HSS2, we also probed the interactions upstream of the core region. With our HSS map as a guide (Fig. 3), the new primer set of oligos 45, 44, and 43 was used sequentially in the LMPCR footprinting protocol. The results of this experiment are shown in Fig. 8. Plasma cell-specific footprints were identified within a novel G-C-rich region at G-298, G-299, and G-302 to 306. This site has not previously been identified as a factor-binding site. While pro- and pre-B-cell lines BASC6C2 and 300-19P-S20 and mature B-cell line BALB1427 showed no footprints within this region (lanes 1 to 3), WEHI231 exhibited part of the protection at G-298 and G-299 (lane 4). This result is consistent with the observation of DNase I hypersensitivity upstream of the core region in WEHI231 (Fig. 2B) and suggests that this cell line has initiated the transition into type L chromatin. Since this new site resides in the middle of HSS1 and HSS2 and since no further footprints were detected with this set of primers nor within a further 170 bp upstream in the complementary strand, these results suggest that interactions at this G-C-rich sequence are involved in the formation of HSS1 and HSS2 in plasma stage cells.

A BSAP-like factor binds the DR-DS junction. Nuclear factors involved in the κE3′ chromatin change would provide valuable insight into the function of this enhancer. The factor(s) that binds the DR-DS junction is most interesting, since its apparent dissociation coincides with the type E to type L switch. To identify this factor, we conducted mobility shift analysis of nuclear extracts isolated from various cell lines by using a sequence of the DR-DS junction (nucleotides 413 to 438) as the probe (oligo DP in Fig. 9A). The result of this analysis, shown in Fig. 9B, indicates the formation of a B-cell-specific complex (arrow) between DP and a factor present in pro-B-cell line BASC6C2, in pre-B cells, and in mature B cells. However, this factor was not detected in plasma cells, the early progenitor cell line LyD9, or non-B-cell line EL4. A faster-moving complex observed in BASC6C2 (Fig. 9B) turned out to

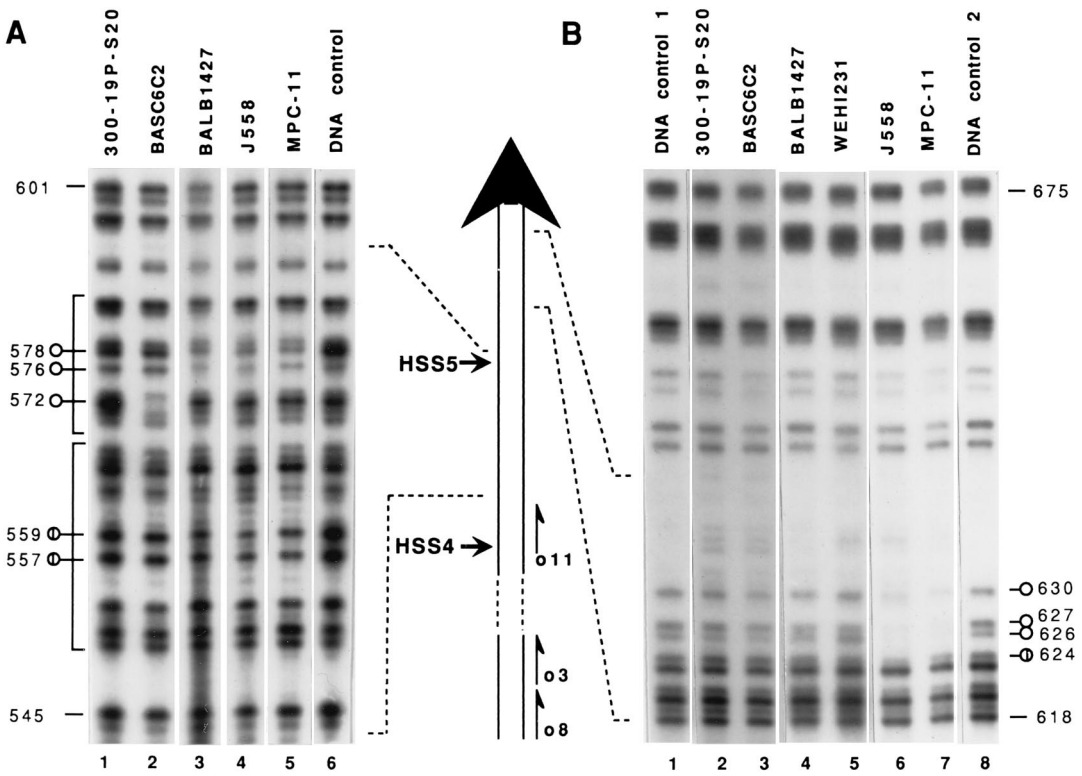

FIG. 7. In vivo methylation pattern in the lower strand within (A) and farther downstream (B) of the HSS4-to-HSS5 region. Cultured cells or naked genomic DNAs (DNA controls) were treated with DMS. The DNA methylation patterns were analyzed by the LMPCR protocol utilizing the primer set of oligos 8, 3, and 11. The names of the cultured cell lines are indicated above the lanes, and their descriptions are given in Table 1. DNA controls were obtained from P388D1 cells for panel A and from 38B9 (control 1) and P388D1 (control 2) cells for panel B. Open circles denote full guanine (G) protection, while slashed circles indicate partial G protection. Beside each symbol or marker is the corresponding nucleotide number of the G residue on the enhancer sequence. In the middle is a schematic diagram of the enhancer showing the approximate locations of HSSs and the sites of hybridization of the oligo primers.

be a proteolytic derivative of the higher DP complex. The cell type distribution of the DP-binding factor is consistent with our in vivo footprinting data (Fig. 5) and resembles the expression pattern of the factor BSAP (9).

BSAP was originally identified as the mammalian homolog of sea urchin histone gene transcription factor TSAP (9) and binds the regulatory region of several B-cell-specific genes (34, 36, 51, 66). BSAP belongs to the PAX family of paired-domain proteins (1) which share a degenerate consensus binding site in DNA (Fig. 9A) (17). We noted a strong similarity (identity at 12 of 14 positions) between the DP sequence and the BSAP consensus sequence (underlined bases in Fig. 9A). To determine whether BSAP or a member of this family of PAX proteins binds DP, we utilized the histone gene promoter sequence H2A2.2, a well-characterized BSAP-binding site (Fig. 9A) (9, 17), as a competitor in the gel shift assay. Figure 9C shows that a 100-fold excess of unlabeled H2A2.2 was able to compete for binding as well as DP itself (competitor lanes marked DP and H2A in bracketed region DP). On the other hand, oligos containing binding sites for transcription factors PU.1 and E-box proteins were unable to compete (lanes marked PU.1 and E box). These results demonstrate that the DP-binding factor recognizes similar binding sites in H2A2.2 and binds in a sequence-specific manner. To further determine the binding site requirements, we investigated the importance of the in vivo-footprinted DP residues by testing mutant oligos in competition experiments. Mutation of DP at positions 419 (C to T) and 423 (G to A) significantly diminished the ability of mutant oligo DPm1 to compete, while mutation of nucleo-

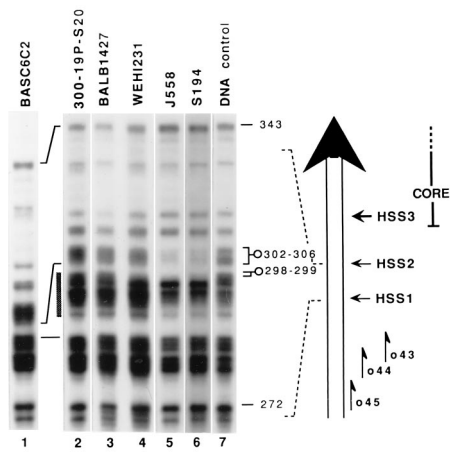

FIG. 8. In vivo methylation pattern in the lower strand of the HSS1-to-HSS2 region. Cultured cells or naked genomic DNAs (DNA control) were treated with DMS and analyzed by the LMPCR protocol by utilizing the primer set of oligos 45, 44, and 43. The names of the cultured cell lines are indicated above the lanes, and their descriptions are given in Table 1. Control DNA was obtained from S194 cells. In this region of the genome, BASC6C2 harbored what appeared to be a polymorphic deletion in the region indicated by the checkered bar. Open circles denote full guanine (G) protection. Beside each symbol or marker is the corresponding nucleotide number of the G residue on the enhancer sequence. On the right is a schematic diagram of the enhancer showing the core region, HSSs, and the sites of hybridization of the oligo primers.

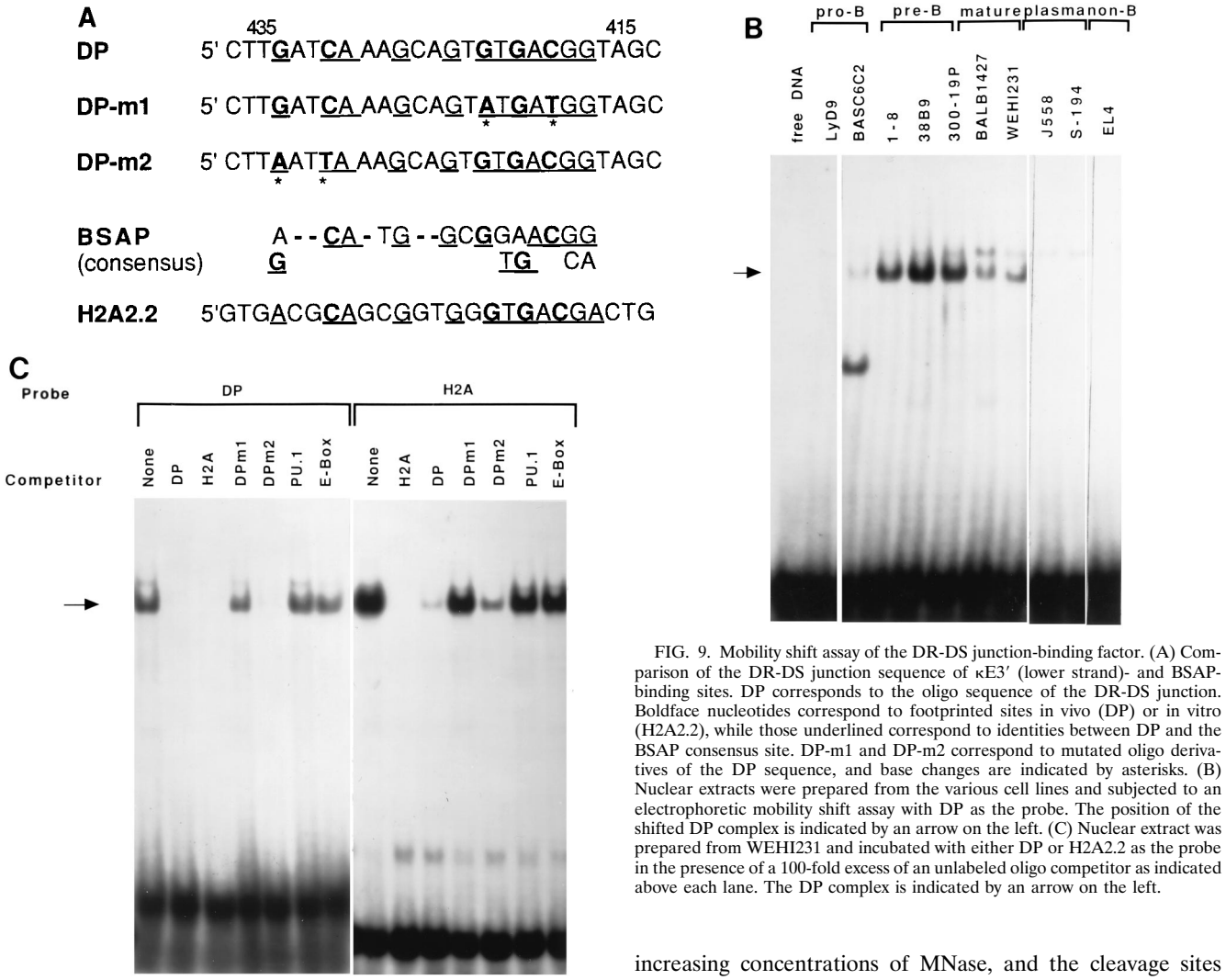

FIG. 9. Mobility shift assay of the DR-DS junction-binding factor. (A) Comparison of the DR-DS junction sequence of κE3′ (lower strand)- and BSAP-binding sites. DP corresponds to the oligo sequence of the DR-DS junction. Boldface nucleotides correspond to footprinted sites in vivo (DP) or in vitro (H2A2.2), while those underlined correspond to identities between DP and the BSAP consensus site. DP-m1 and DP-m2 correspond to mutated oligo derivatives of the DP sequence, and base changes are indicated by asterisks. (B) Nuclear extracts were prepared from the various cell lines and subjected to an electrophoretic mobility shift assay with DP as the probe. The position of the shifted DP complex is indicated by an arrow on the left. (C) Nuclear extract was prepared from WEHI231 and incubated with either DP or H2A2.2 as the probe in the presence of a 100-fold excess of an unlabeled oligo competitor as indicated above each lane. The DP complex is indicated by an arrow on the left.

tides 432 (C to T) and 435 (G to A) had no effect on the ability of mutant oligo DPm2 to compete at 100-fold excess. This result suggests that the nucleotides at positions 419 and 423 are more important for binding in vitro. Interestingly, utilization of H2A2.2 as a labeled probe in competition experiments showed a complex with the same mobility and the same binding properties as the DP complex (bracketed lanes marked H2A). That is, DP, H2A2.2 itself, and DPm2 were able to compete with H2A2.2 for binding, but DPm1, PU.1, and E-box oligos were not. These cross-competition data (Fig. 9C), combined with strong binding site (Fig. 9A) and expression pattern (Fig. 9B) similarities between the DP-binding factor and BSAP, suggest that BSAP or a member of this family of PAX proteins binds the κE3′ DP sequence and could play a role in the chromatin structural change in vivo.

Nucleosomes rearrange during the transition from type E type L chromatin. Full understanding of the role of nuclear factors in the induction of chromatin change requires knowledge of their binding in the context of nucleosomes. To better elucidate the nature of the chromatin transition between type E and type L, we examined the nucleosomal organization at E3′. To do this, we utilized the enzyme MNase, which cleaves the DNA backbone in the linker region between nucleosomes. Cells were permeabilized with lysolecithin and incubated with increasing concentrations of MNase, and the cleavage sites were mapped with respect to the downstream *Bgl*II site as shown in Fig. 1A. Since MNase exhibits a preference for certain sequences in DNA (32), protein-free genomic DNA and non-B-cell line EL4 were also subjected to the same procedure as controls. The results are shown in Fig. 10A and are interpreted in a nucleosomal map in Fig. 10B. Faint cleavage sites were observed in naked DNA, reflecting the enzyme's sequence specificity. A similar but more pronounced cutting pattern was evident in non-B-cell line EL4 (checkered circles). The EL4 pattern could result from the enzyme's sequence preference or the phasing of nucleosomes in this non-B-cell line. Although we could not distinguish between these two possibilities, these data proved to be a useful reference for interpreting the results obtained with the B-cell lines. BASC6C2 and BALB1427 (Fig. 10A) and pre-B-cell line 300-19P (data not shown) exhibited similar MNase digestion patterns. Two strong cleavage sites were mapped to positions 390 and 480 (±30 bp) within the core region (arrows in Fig. 10A and B). Because this interval is too short to accommodate a nucleosome, these sites likely approximate the borders of a nonnucleosomal protein complex. This interpretation is consistent with data showing accessibility of this region to DNase I and with the observed major-groove protection of factor-binding sites within this region (Fig. 2 and 5). Other cleavage sites were identified at positions 190, 560, 760, and 910 ± 30

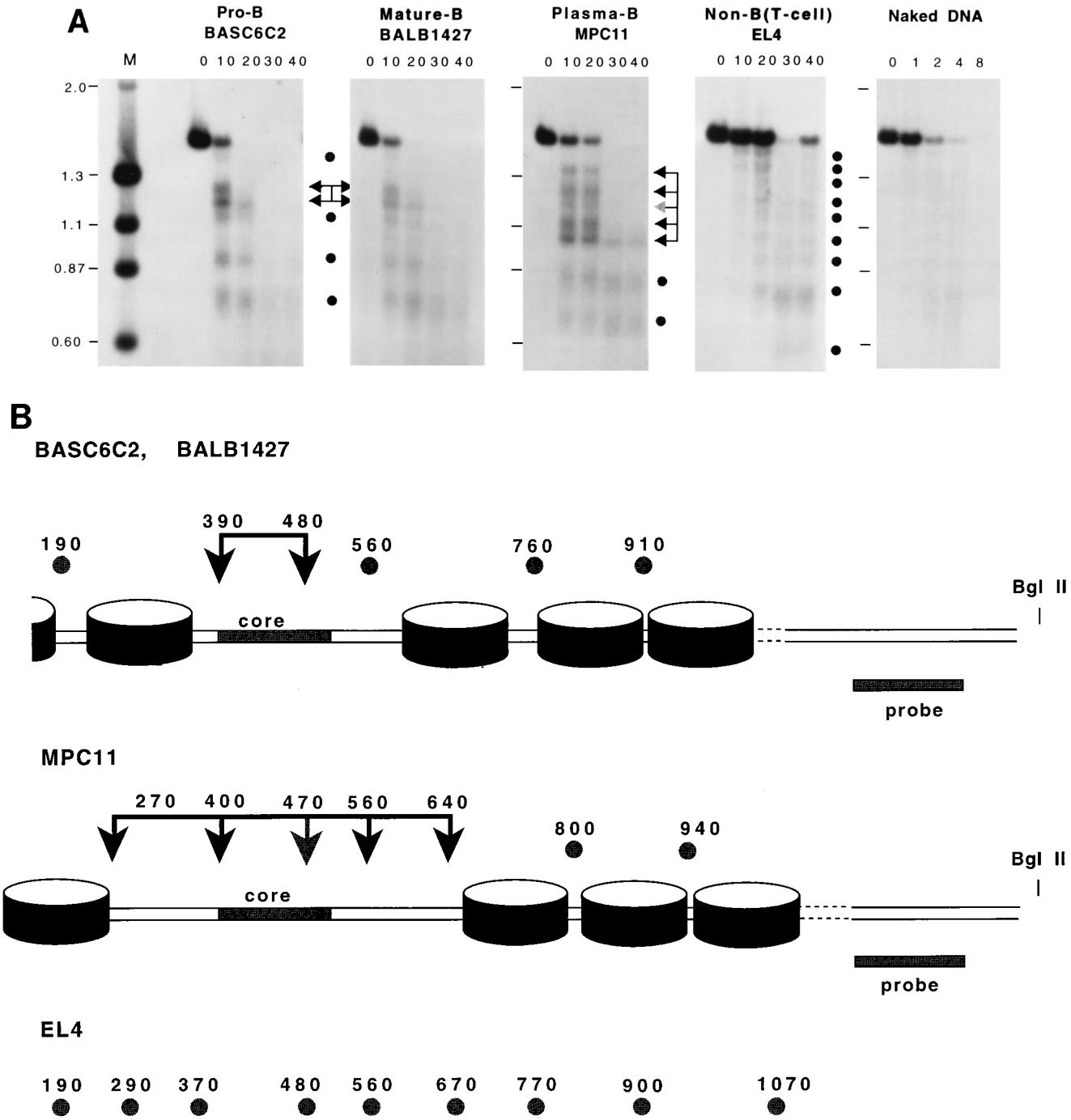

FIG. 10. (A) MNase digestion analysis of E3′ chromatin. Cell lines were permeabilized with lysolecithin and treated with various concentrations of MNase. After enzyme treatment, DNA was purified, cut with *Bgl*II, and analyzed on a Southern blot by indirect end labeling as described in the legend to Fig. 1A. Arrows indicate the positions of strong MNase cuts. Stippled circles indicate likely boundaries of nucleosomes. Lane M contained markers 2.0, 1.3, 1.1, 0.87, and 0.60 kb long, whose migration positions are indicated by short horizontal bars adjacent to the various gels. (B) Map of the MNase cut sites in BASC6C2, BALB1427 (pro-B and mature B cells), MPC11 (plasma cells), and EL4 (non-B cells) cells with an error of ±30 bp. MNase cleavage sites within E3′ were determined as described in the legend to Fig. 2. Average sizes of the MNase-cleaved fragments were 1,500, 1,280, 1,200, 1,120, 920, and 760 bp for BASC6C2 and BALB1427 cells and 1,360, 1,240, 1,170, 1,080, 990, 840, and 700 bp for MPC11 cells. For EL4 cells, fragment lengths were determined to be 1,500, 1,390, 1,310, 1,200, 1,120, 1,010, 920, 780, and 610 bp. Cylindrical disks represent proposed nucleosomal positions.

(checkered circles). Notably, positions 290 and 670, which were accessible in EL4 chromatin, were inaccessible in BASC6C2 and BALB1427, preserving a 200-bp MNase-resistant interval between positions 190 and 390 and between positions 560 and 760. Since this interval is large enough to accommodate a nucleosome, these data suggest the presence of specifically positioned nucleosomes flanking the core region (Fig. 10B). This interpretation is substantiated by the observation of a nucleosomal ladder when the MNase digests were analyzed directly with appropriate probes on a Southern blot (data not

shown). Cleavage sites at 760 and 910 also likely reflect the presence of a nucleosome as opposed to mere MNase sequence preference, since the same sites were cleaved by DNase I in WEHI231 chromatin (Fig. 2B, lane 2, and data not shown).

In plasma cell line MPC11, a different cutting pattern was observed. MNase cleaved over a larger area with strong cutting sites at positions 270, 400, 560, and 640 ± 30 (bracketed arrows in Fig. 10A). The originally strong cleavage site at position 480 in BASC6C2 and BALB1427 cells (lower arrow in Fig. 10A) was suppressed in MPC11 cells (crosshatched arrow). These results suggest a change in protein-DNA interactions at the core and flanking regions consistent with the DNase I and in vivo footprinting data. Cleavage at positions 270 and 640 likely reflects the external boundaries of the type L-specific protein complex assembled at E3′ but also suggests the displacement or repositioning of nucleosomes flanking the core in type E chromatin. Cleavage sites at positions 760 and 910 in BASC6C2 and BALB1427 cells (checkered circles) were also shifted 30 to 40 bp downstream to positions 800 and 940 in MPC11 cells, and that at position 190 could not be detected in MPC11 cells. These data are consistent with the interpretation that precisely positioned nucleosomes flanking the core region rearrange during the transition from type E to type L chromatin (Fig. 10B). Thus, changes in chromatin structure at E3′ between the mature and plasma B-cell stages can be explained not only by a switch in the composition of bound nuclear factors but also by the rearrangement of nucleosomes.

DISCUSSION

To gain insight into the function of κE3′, we characterized its chromatin structure in B-cell lines arrested at different stages of development. Our studies revealed two patterns of chromatin organization within this region: type E, which occurs in pro-B, pre-B, and mature B cells, and type L, which was found in plasma stage cells. In type E chromatin, DNase I hypersensitivity was localized to a 120-bp contiguous area of the core region. This pattern of accessibility coincided with guanosine protection at the DR-DS, PU.1–NF-EM5, and E box 1 sites. Since these in vivo footprints agree with the protection patterns exhibited by nuclear factors ATF-1–CREM, BSAP, PU.1–NF-EM5, and E2A in vitro (31, 57–59; this work), these results suggest that these nuclear proteins play a role in the establishment of the early exposed chromatin structure. The occurrence of these footprints at the pro- and pre-B-cell stages further indicates that these factors bind κE3′ prior to kappa gene rearrangement. Because most of the pro-B-cell lines studied do not produce cytoplasmic μ (Table 1) (30), it appears that type E formation also precedes μ expression.

In type L chromatin, DNase I hypersensitivity extended to regions upstream and downstream of the initial site, resulting in the appearance of five distinct HSSs: HSS1 to HSS5. This new chromatin arrangement was found only in plasma stage cells and correlated with increased kappa transcription, although its formation was not limited to kappa chain-producing cells (Table 1). Lambda producers that maintained a transcriptionally active kappa locus exhibited the same structure. The chromosomal alteration was observed in both IgM-producing and class-switched secretors and was not dependent upon ongoing immunoglobulin secretion. These results indicate that the observed chromatin transition depends solely upon the differentiation state of the cell. Localization of type L chromatin to factor-binding sites indicated that among the early sites, only PU.1–NF-EM5 and E box 1 remained unequivocally occupied at the plasma cell stage. Partial protection at the upstream region of DR, reported to bind ATF-1 and CREM, was also detected, although the developmental specificity of these interactions is unclear since the most intense footprints occurred in WEHI 231, a mature B-cell line. Three changes in protein-DNA interactions correlate with the type E to type L chromatin transition: (i) disappearance of protection at the DR-DS junction, (ii) appearance of protection upstream at a G-C-rich sequence within HSS1 and HSS2, and (iii) appearance of protection downstream at the NF-E1 binding site. The formation of type L chromatin therefore correlates with a switch in the composition of bound factors.

Footprints were also detected that did not obviously correlate with stage-specific chromatin structures (Fig. 5B). In type E chromatin, these protections were found mostly outside the E3′ core within a region that was found to repress transcriptional function at the pre-B-cell stage. We observed a strong footprint at G-572 and partial footprints at G-549 and G-562 in pro-B-cell line BASC6C2. The identity of the factors responsible for these footprints is unknown. On the other hand, we did not detect footprints at the binding sites for NF-E1 (positions 624 to 630) or LEF-1 (positions 529 to 540) in BASC6C2, 300-19P-S20, and all of the other pro-B- and pre-B-cell lines studied (data not shown). Binding of LEF-1 was expected to protect G-532 and 533, residues extrapolated to be the major-groove contact sites of this protein on the basis of in vitro studies (40, 70). It is important to note, however, that LEF-1 engages DNA mainly in the minor groove (23) and interactions such as these are not detected by DMS. The use of probes with different specificity should shed further light on the binding of this protein. Finally, footprints at two E boxes downstream (E boxes 2 and 3) were detected in mature and plasma stage cells but not in earlier-stage cells. The absence of NF-E1 and E-box 2 and 3 footprints in pro- and pre-B cells could be explained by constraints imposed by chromatin structure and is discussed further below.

A model of κE3′ chromatin structure during B-cell development. MNase digestion analysis revealed a nucleosomal organization at E3′ that was largely consistent with the DNase I hypersensitivity and in vivo footprinting data. This allowed us to fit our observations into a working model of κE3′ chromatin structure during development (Fig. 11). This model integrates our findings (Fig. 2, 5, and 10) with existing factor-binding information in the literature (31, 40, 53, 57–59). At the early B-cell stage, PU.1–NF-EM5, E12/E47-like complexes, the DR-binding complex, and a BSAP-like protein bind to E3′ in a B-cell-specific manner, excluding nucleosomes from the core region and creating the type E early hypersensitive structure. The presence of this core complex results in the precise positioning of nucleosomes at flanking sites which, in turn, potentially interfere with the binding of other factors. For example, the nucleosomal nature of the downstream region likely interferes with the ability of ubiquitous NF-E1 to bind at the early stage, explaining the absence of NF-E1 footprints in pro-B, pre-B, and mature B cells in vivo (Fig. 7B). While our results make an NF-E1 role at the early B-cell stage unlikely, we have not been able to identify extensively footprinted residues in pro- or pre-B cells to explain the negative transcriptional role of this downstream region in early B cells (53) apart from the few footprints in BASC6C2 discussed above. Type E chromatin is maintained at the mature B-cell stage with a few changes in its footprinting pattern, which includes the occupancy of E boxes 2 and 3, and later, the apparent binding of a G-C-rich sequence-specific factor upstream. We hypothesize that transition into type L chromatin at the plasma stage is generated by concomitant changes in both the binding of sequence-specific factors and the rearrangement of nucleosomes. Our simplest interpretation of type L chromatin HSS1 through HSS5 is as

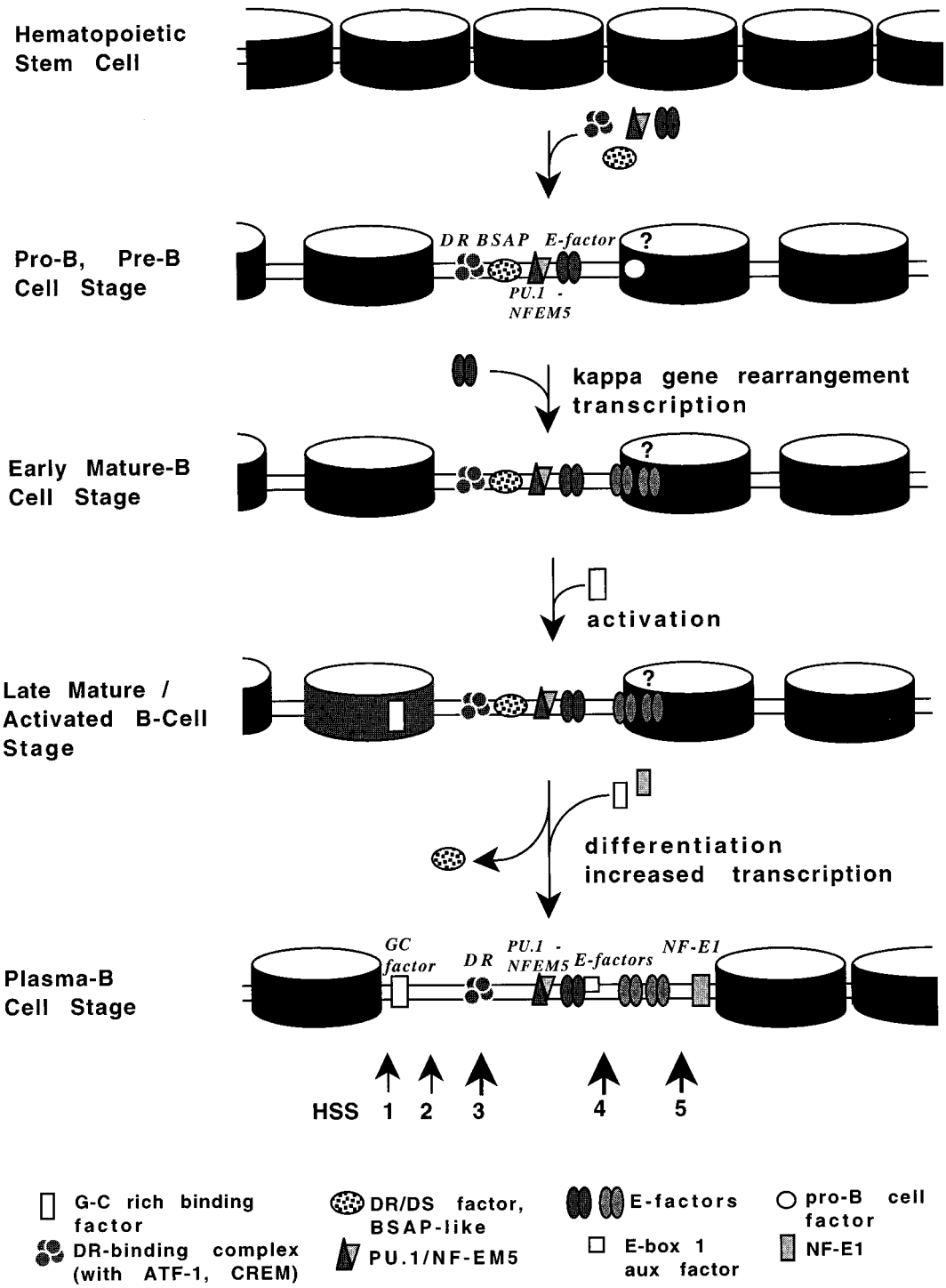

FIG. 11. Model of κE3′ chromatin structure during B-cell development. Cylindrical disks represent nucleosomes, while smaller geometric figures represent nonhistone protein factors as identified at the bottom. Filled geometric patterns represent factors that have been characterized in vitro, while open patterns represent unidentified or uncharacterized factors. Lightly shaded nucleosomes might possess a structure different from that of the normal, darkly shaded ones. The arrows at the bottom indicate the approximate locations of HSSs in type L chromatin.

follows. Dissociation of a BSAP-like factor that binds the DR-DS junction alters protein-DNA interactions at this region, inducing HSS3. The binding of a GC-rich-specific factor(s) upstream of the core region displaces a nucleosome, generating HSS1 and HSS2. Finally, the plasma stage-specific binding of an NF-E1-like factor displaces the flanking nucleosome downstream, inducing HSS4 and HSS5. The causal relationship between the dissociation of a BSAP-like factor at the core region and the binding of factors upstream and downstream remains to be investigated. It also remains to be ana-

lyzed whether the structure and composition of nucleosomes vary between B-cell stages, facilitating the observed changes in interactions, and whether additional sequence-specific factors not detected by DMS footprinting are involved in this process. Why no distinctive change in the type E hypersensitivity pattern is induced by the occupancy of E boxes 2 and 3 at the mature B-cell stage is not clear. An interesting possibility is that these factors are able to bind their cognate sites without displacement of a nucleosome (shown in Fig. 11). Increasing evidence supports this possibility (2, 39). Elucidation of the nucleosomal nature of these binding sites at the nucleotide sequence level should shed further light on this question.

In addition to the two basic configurations of chromatin at E3′, the structure observed in WEHI231 could represent a transitional state between type E and type L, a state represented in Fig. 11 as the mature activated B-cell stage. In this configuration, DNase I hypersensitivity extends upstream but not downstream of the core (Fig. 2). This chromatin alteration was localized to two protected guanosine residues, a subset of the same G-C-rich region that was completely protected in plasma stage cells (Fig. 8). We interpret this to indicate the binding of a G-C-rich sequence-specific factor which may or may not be the same factor that binds at the plasma stage. The nucleosome at this site may be perturbed, as evidenced by the altered pattern of DNase I hypersensitivity (Fig. 11). These data suggest that WEHI231 chromatin has progressed slightly beyond the basic type E and lends credence to the developmental relatedness of type E and type L chromatin. The placement of WEHI231 at this stage in the B-cell pathway is consistent with recent studies of its developmental state (26). The analysis of additional mature B-cell lines representing more advanced stages should enable us to confirm the generality of this intermediate state and reconstruct the sequence of events leading to type L chromatin.

Although our results invoke an early role for PU.1–NF-EM5, E12/E47, the DR-binding complex, and BSAP-like factors in the activation of κE3′, the molecular details of this event are unclear. For example, we do not know whether these factors bind in a concerted or sequential fashion and, if they bind sequentially, which of these factors binds first. LyD9 was the only progenitor B-cell line tested which failed to show chromatin alterations at the 3′ enhancer (Table 1). This cell line also failed to reveal any in vivo footprints (data not shown). LyD9 is an interleukin 3-dependent multipotential clone with early lymphomyeloid progenitor characteristics (52). Studies of this cell line revealed a lack of E-box DNA-binding activity which correlated inversely with the expression of Id mRNA (47, 74). On the other hand, more advanced pro-B-cell lines which downregulated Id mRNA (e.g., BASC6C2) exhibited E-factor DNA-binding activity (74). Although the state of PU.1–NF-EM5 and DR-binding factors in LyD9 is unknown, the lack of E-factor DNA-binding activity correlates with this cell line's inability to open up its κE3′ chromatin (Table 1) and suggests an important role for E factors in setting up the initial chromatin alteration. This is consistent with the recent demonstration that the knockout of E2A (E12/E47) function interferes with lymphoid differentiation at an early stage (8, 68, 79) and identifies κE3′ as an early target for this factor. The characterization of a chromatin structure in pro-B cells representing an intermediate stage between those of LyD9 and BASC6C2 cells or those derived from viable knockout mice whose genes for specific transcription factors have been abolished, e.g., E2A null mutants (8, 79), should provide further insight into the early events that activate E3′.

Candidate nuclear factors involved in the type E to type L chromatin transition. The identification of nuclear factors involved in the κE3′ chromatin change is important in the delineation of this enhancer's function. Our identification of BSAP or a BSAP-like factor as one such protein provides interesting new insights into the role of κE3′ during B-cell development. The interaction of BSAP with the DR-DS junction may have been missed in previous investigations because the factor-binding abilities of the DR and downstream sites have often been studied separately (31, 58). The exclusion of constitutive factor-binding sites in our design of the DP oligo (DR-DS gel shift probe) may have also helped to simplify the gel shift pattern obtained. BSAP is expressed in pro-B, pre-B, and mature B cells but not in plasma cells (1, 9), an expression pattern that mirrors the stage-specific occupancy of the DR-DS junction. BSAP binding sites have been identified 5′ of IgH switch regions and within IgH αE3′ (36, 66), promoters of the CD19 gene (34), and V_{preB1} (51). The BSAP consensus site is not only strongly similar to the κE3′ DR-DS junction sequence; the contact sites of BSAP with DNA in vitro (17) also coincide with four of the five footprinted G residues at the κE3′ site in vivo (boldface letters in DP and H2A2.2 in Fig. 9A). We hypothesize that our in vivo footprints at nucleotide positions 419 to 423 and those at 432 to 435 constitute the two halves of the proposed bipartite recognition sequence of BSAP (17). It has been proposed that both contact sites could make similar contributions to the overall affinity or one of the two contact sites might dominate over the other (17). The latter case appears to be true for the binding of the BSAP-like factor to DP, with half-site G contacts at positions 419 and 423 appearing to be more important for binding than G contacts at positions 432 and 435 (Fig. 9C). Overall, our demonstration of the remarkable similarity between the DP-binding factor and BSAP suggests that BSAP or a related PAX protein binds κE3′ and likely plays a pivotal role in the type E to type L chromatin switch.

Inspection of the plasma stage-specific footprints of type L chromatin revealed interesting similarities with binding sites for known transcription factors. The G-C-rich sequence within HSS1 and HSS2 resembles the consensus site for Zn finger proteins SP1 and H4TF1 (21). Curiously, both Zn finger proteins are ubiquitous (21). While this upstream factor remains to be identified, the downstream site that we invoked in the formation of HSS4 and HSS5 binds NF-E1, also a Zn finger protein and also ubiquitous. Although it was previously demonstrated that NF-E1 could repress transcription (53), our data are more consistent with the notion that NF-E1 functions as a positive regulator of E3′ function. Indeed, the NF-E1 primary structure suggests a bifunctional protein capable of both positive and negative transcriptional effects (28, 53). Further studies are necessary to assess the role of the NF-E1 site at the plasma stage.

Footprints downstream of the core region at E boxes 2 and 3 suggest the binding of helix-loop-helix factors (46) at the mature and plasma cell stages but not at the pro-B-cell stage. It was recently demonstrated that E12/E47-like factors indeed bind these sites in vitro (40). It is not clear whether the same E factors bind E boxes 1, 2, and 3. How each of these sites impacts upon the structure and function of E3′ chromatin at the early, mature, and plasma stages awaits the identification and elucidation of the bound factors.

Functional implications of chromatin structure. The occupancy of E3′ by factors prior to active transcription of the kappa gene mirrors the inducible state of genes like PHO5 and GAL1 to GAL10 in *Saccharomyces cerevisiae* and the human and drosophila heat shock promoters (reviewed in reference 72). Since PU.1, E factors, and even BSAP were originally identified as transcription factors, their role at the early B-cell

stage in the context of an unrearranged kappa gene is not clear. They may be involved in regulating germ line transcription, a process postulated to be necessary for gene rearrangement (64, 71, 76). Indeed, transcription from a thymidine kinase gene promoter is supported by the E3′ core region in pre-B cells, and both the PU.1- and E12/E47-binding sites appear to contribute to this process (53, 58). On the other hand, transcription-repressive effects have also been observed when intact E3′ was included in a construct containing the germ line promoter and the kappa intronic enhancer (22). Because recombination constructs containing the intronic enhancer but lacking E3′ exhibited precocious kappa gene rearrangement in transgenic mice (24), it has been hypothesized that E3′ might function to prevent gene rearrangement by suppressing germ line transcription at the early stage (22). This possibility has gained support by the recent demonstration via transgenic mouse experiments that κE3′ regulates the B-cell versus T-cell specificity and stage specificity of kappa gene rearrangement (29). While the PU.1-binding site has been shown to play a role in this process (29), the role of the other early factor-binding sites that we detected in type E chromatin remains to be tested. A possibility not mutually exclusive of the preceding scenarios is that these early factors serve to open up sites in chromatin, establishing a locus that is accessible to the recombination or suppressive apparatus at the early stage and the transcriptional apparatus at the later stage. These factors may perform versatile roles by being able to interact with components of either type of protein complex. The knockout of this enhancer should shed further light on the role of an open E3′ chromatin at the early stage.

The faultless differentiation dependence of the chromatin switch from type E to type L is intriguing and must have functional consequences for the role of κE3′. This structural switch might be necessary to upregulate kappa transcription during terminal differentiation. A similar function in IgH transcription has been proposed for heavy-chain αE3′ (18, 50). Although sequences outside of the core region have not been shown to contribute significantly to transcription at the plasma stage (31, 42, 57), this information was obtained by deletional analysis which may not adequately reflect interactions among factors bound at distant sites. Our results necessitate a reevaluation of the role of these flanking sites in the context of an intact enhancer sequence in both transient and stable transfection assays. It is also important to note that potentially repressive effects associated with the type E complex have not been explored. The determination of the role of the DR-DS junction (BSAP-binding site) at the early and mature B-cell stages could shed light on this question. In fact, BSAP has been shown to repress IgH αE3′ activity in mature B cells (50, 66) via exclusion of the binding of another factor downstream (49) and might function in a similar capacity at κE3′. The involvement of BSAP in the regulation of both heavy- and light-chain genes might be necessary to coordinate transcription at the two loci prior to terminal differentiation. Another possible role for the type E to type L structural switch might be in somatic hypermutation. E3′ has been shown to play a role in this process in transgenic mouse experiments (10). Although this phenomenon has not been demonstrated to occur in cultured cell lines, it would be interesting to know whether a subset of the factors detected in vivo might participate in this event.

DNase I-hypersensitive sites have historically been useful in defining important DNA sequences that had no apparent function when first discovered (25). The approach utilized in this study enabled us to identify potentially important sequences within and flanking the E3′ core region not detected previously by transcriptional approaches or gel shift analysis and whose functional significance might only be clearly manifested in the context of chromatin. The information derived here should complement that obtained by analysis of factors that bind enhancer sequences in vitro. Our chromatin model provides a conceptual framework with which the role of already identified factors could be reexamined and the role of new factors could be uncovered. Finally, the revelation of an E3′ nucleoprotein structure that changes with the functional state of the kappa gene is intriguing and suggests that this enhancer plays more than one role in kappa gene regulation. We suggest that a crucial switch in κE3′ function occurs in the mature cell to plasma cell transition.

ACKNOWLEDGMENTS

We thank N. Rosenberg, D. Baltimore, F. Alt, J. Pierce, H. Morse, R. Palacios, T. Kinashi, M. Reth, M. Xu, and P. Tucker for gifts of cell lines. We thank W. T. Garrard for critical reading of the manuscript and D. Stauffer, J. Wilberding, and R. Mallorca in our laboratory for helpful discussions.

This work was supported in part by an endowment from the Galla family to the University of Notre Dame and in part by NIH grant GM-51165 to V.B.

REFERENCES

1. **Adams, B., P. Dorfler, A. Aguzzi, Z. Kozmik, P. Urbanek, I. Maurer-Fogy, and M. Busslinger.** 1992. Pax-5 encodes the transcription factor BSAP and is expressed in B-lymphocytes, the developing CNS, and adult testis. Genes Dev. **6:**1589–1607.
2. **Adams, C. C., and J. L. Workman.** 1993. Nucleosome displacement in transcription. Cell **72:**305–308.
3. **Alt, F., G. Yancopoulos, T. Blackwell, C. Wood, E. Thomas, M. Boss, R. Coffman, N. Rosenberg, S. Tonegawa, and D. Baltimore.** 1984. Ordered rearrangement of immunoglobulin heavy chain variable region segments. EMBO J. **3:**1209–1219.
4. **Alt, F. W., T. K. Blackwell, and G. D. Yancopoulos.** 1987. Development of the primary antibody repertoire. Science **238:**1079–1087.
5. **Alt, F. W., N. Rosenberg, V. Enea, E. Siden, and D. Baltimore.** 1982. Multiple immunoglobulin heavy-chain gene transcripts in Abelson murine leukemia virus-transformed lymphoid cell lines. Mol. Cell. Biol. **2:**386–400.
6. **American Type Culture Collection.** 1992. Catalogue of cell lines and hybridomas, 7th ed. American Type Culture Collection, Rockville, Md.
7. **Atchison, M. L., and R. P. Perry.** 1987. The role of the κ enhancer and its binding factor NFκB in the developmental regulation of κ gene transcription. Cell **48:**121–128.
8. **Bain, G., E. C. R. Maandag, D. J. Izon, D. Amsen, A. M. Kruisbeek, B. C. Weintraub, I. Krop, M. S. Schlissel, A. J. Feeney, M. van Roon, M. van der Valk, H. P. J. te Riele, A. Berns, and C. Murre.** 1994. E2A proteins are required for proper B-cell development and initiation of immunoglobulin gene rearrangements. Cell **79:**885–892.
9. **Barberis, A., K. Widenhorn, L. Vitelli, and M. Busslinger.** 1990. A novel B-cell lineage-specific transcription factor present at early but not late stages of differentiation. Genes Dev. **4:**849–859.
10. **Betz, A. G., C. Milstein, A. Gonzalez-Fernandez, R. Pannell, T. Larson, and M. S. Neuberger.** 1994. Elements regulating somatic hypermutation of an immunoglobulin κ gene: critical role for the intron enhancer/matrix attachment region. Cell **77:**239–248.
11. **Blasquez, V. C., M. A. Hale, K. W. Trevorrow, and W. T. Garrard.** 1992. Immunoglobulin κ gene enhancers synergistically activate gene expression but independently determine chromatin structure. J. Biol. Chem. **267:**23888–23893.
12. **Blasquez, V. C., M. Xu, S. C. Moses, and W. T. Garrard.** 1989. Immunoglobulin κ gene expression after stable integration. I. Role of the intronic *MAR* and enhancer in plasmacytoma cells. J. Biol. Chem. **264:**21183–21189.
13. **Bradford, M. M.** 1976. A rapid and sensitive method for the quantitation of microgram quantities of protein utilizing the principle of protein-dye binding. Anal. Biochem. **72:**248–254.
14. **Brooks, K., D. Yuan, J. W. Uhr, P. H. Krammer, and E. S. Vitetta.** 1983. Lymphokine-induced IgM secretion by clones of neoplastic B cells. Nature (London) **302:**825–826.
15. **Chen-Bettecken, U., E. Wecker, and A. Schimpl.** 1987. Transcriptional control of μ- and κ-gene expression in resting and bacterial lipopolysaccharide-activated normal B-cells. Immunobiology **174:**162–176.
16. **Contreras, R., and W. Fiers.** 1981. Initiation of transcription by RNA polymerase II in permeable SV40-infected CV-1 cells; evidence for multiple promoters of SV40 late transcription. Nucleic Acids Res. **2:**215–236.
17. **Czerny, T., G. Schaffner, and M. Busslinger.** 1993. DNA sequence recogni-

tion by Pax proteins: bipartite structure of the paired domain and its binding site. Genes Dev. **7:**2048–2061.
18. **Dariavach, P., G. T. Williams, K. Campbell, S. Pettersson, and M. S. Neuberger.** 1991. The mouse IgH 3′-enhancer. Eur. J. Immunol. **21:**1499–1504.
19. **Davidson, W. F., J. H. Pierce, S. Rudikoff, and H. C. Morse.** 1988. Relationships between cell and myeloid differentiation, studies with a B-lymphocyte progenitor line, HAFTL-1. J. Exp. Med. **168:**389–407.
20. **Dignam, J. D., R. M. Lebovitz, and R. Roeder.** 1983. Accurate transcription initiation by RNA polymerase II in a soluble extract from isolated mammalian nuclei. Nucleic Acids Res. **11:**1475–1489.
21. **Faisst, S., and S. Meyer.** 1992. Compilation of vertebrate-encoded transcription factors. Nucleic Acids Res. **20:**3–26.
22. **Fulton, R., and B. Van Ness.** 1993. Kappa immunoglobulin promoters and enhancers display developmentally controlled interactions. Nucleic Acids Res. **21:**4941–4947.
23. **Giese, K., J. Cox, and R. Grosschedl.** 1992. The HMG domain of lymphoid enhancer factor 1 bends DNA and facilitates assembly of functional nucleoprotein structures. Cell **69:**185–195.
24. **Goodhardt, M., C. Babinet, G. Lufalla, S. Kallenbach, P. Cavelier, and F. Rougeon.** 1989. Immunoglobulin κ light chain gene promoter and enhancer are not responsible for B-cell restricted gene rearrangement. Nucleic Acids Res. **17:**7403–7415.
25. **Gross, D. S., and W. T. Garrard.** 1988. Nuclease hypersensitive sites in chromatin. Annu. Rev. Biochem. **57:**159–197.
26. **Haggerty, H. G., R. J. Wechsler, V. M. Lentz, and J. G. Monroe.** 1993. Endogenous expression of δ on the surface of WEHI-231. J. Immunol. **9:**4681–4691.
27. **Hardy, R. R., C. E. Carmack, S. A. Shinton, J. D. Kemp, and K. Hayakawa.** 1991. Resolution and characterization of pro-B and pre-pro-B cell stages in normal mouse bone marrow. J. Exp. Med. **173:**1213–1225.
28. **Hariharan, N., D. E. Kelley, and R. P. Perry.** 1991. δ, a transcription factor that binds to downstream elements in several polymerase II promoters, is a functionally versatile zinc finger protein. Proc. Natl. Acad. Sci. USA **88:** 9799–9803.
29. **Hiramatsu, R., K. Akagi, M. Matsuoka, K. Sakumi, H. Nakamura, L. Kingsbury, C. David, R. Hardy, K. Yamamura, and H. Sakano.** 1995. The 3′ enhancer region determines the B/T specificity and pro-B/pre-B specificity of immunoglobulin Vκ-Jκ joining. Cell **83:**1113–1123.
30. **Holmes, K. L., J. H. Pierce, W. F. Davidson, and H. C. Morse III.** 1986. Murine hematopoietic cells with pre-B or pre-B/myeloid characteristics are generated by in vitro transformation with retroviruses containing *fes*, *ras*, *abl*, and *src* oncogenes. J. Exp. Med. **164:**443–457.
31. **Judde, J.-G., and E. E. Max.** 1992. Characterization of the human immunoglobulin kappa gene 3′ enhancer: functional importance of three motifs that demonstrate B-cell-specific in vivo footprints. Mol. Cell. Biol. **12:**5206–5216.
32. **Keene, M. A., and S. C. R. Elgin.** 1981. Micrococcal nuclease as a probe of DNA sequence organization and chromatin structure. Cell **27:**57–64.
33. **Kelley, D. E., and R. P. Perry.** 1986. Transcriptional and posttranscriptional control of immunoglobulin mRNA production during B-lymphocyte development. Nucleic Acids Res. **14:**5431–5447.
34. **Kozmik, Z., S. Wang, P. Dorfler, B. Adams, and M. Busslinger.** 1992. The promoter of the CD19 gene is a target for the B-cell-specific transcription factor BSAP. Mol. Cell. Biol. **12:**2662–2672.
35. **Lenardo, M., J. W. Pierce, and D. Baltimore.** 1987. Protein-binding sites in Ig gene enhancers determine transcriptional activity and inducibility. Science **236:**1573–1577.
36. **Liao, F., S. L. Giannini, and B. K. Birshtein.** 1992. A nuclear DNA-binding protein expressed during early stages of B-cell differentiation interacts with diverse segments within and 3′ of the Ig H chain gene cluster. J. Immunol. **148:**2909–2917.
37. **Liou, H.-C., W. C. Sha, M. L. Scott, and D. Baltimore.** 1994. Sequential induction of NF-κB/Rel family proteins during B-cell terminal differentiation. Mol. Cell. Biol. **14:**5349–5359.
38. **McGhee, J. D., and G. Felsenfeld.** 1979. Reaction of nucleosome DNA with dimethyl sulfate. Proc. Natl. Acad. Sci. USA **76:**2133.
39. **McPherson, C. E., E.-Y. Shim, D. S. Friedman, and K. S. Zaret.** 1993. An active tissue-specific enhancer and bound transcription factors existing in a precisely positioned nucleosomal array. Cell **75:**387–398.
40. **Meyer, K. B., and J. Ireland.** 1994. Activation of the immunoglobulin κ3′ enhancer in pre-B cells correlates with the suppression of a nuclear factor binding to a sequence flanking the active core. Nucleic Acids Res. **22:**1576–1582.
41. **Meyer, K. B., and M. S. Neuberger.** 1989. The immunoglobulin κ locus contains a second, stronger B-cell-specific enhancer which is located downstream of the constant region. EMBO J. **8:**1959–1964.
42. **Meyer, K. B., M. J. Sharpe, M. A. Surani, and M. S. Neuberger.** 1990. The importance of the 3′-enhancer region in immunoglobulin κ gene expression. Nucleic Acids Res. **18:**5609–5615.
43. **Miyamoto, S., M. J. Schmitt, and I. M. Verma.** 1994. Qualitative changes in the subunit composition of κB-binding complexes during murine B-cell differentiation. Proc. Natl. Acad. Sci. USA **91:**5056–5060.
44. **Mueller, P. R., and B. Wold.** 1989. In vivo footprinting of a muscle specific enhancer by ligation mediated PCR. Science **246:**780–786.
45. **Murre, C., P. S. McCaw, and D. Baltimore.** 1989. A new DNA binding and dimerization motif in immunoglobulin enhancer binding, daughterless, MyoD, and myc proteins. Cell **56:**777–783.
46. **Murre, C., P. S. McCaw, H. Vaessin, M. Caudy, L. Y. Jan, Y. N. Jan, C. V. Cabrera, J. N. Buskin, S. D. Hauschka, A. Lassar, H. Weintraub, and D. Baltimore.** 1989. Interactions between heterologous helix-loop-helix proteins generate complexes that bind specifically to a common DNA sequence. Cell **58:**537–544.
47. **Murre, C., A. Voronova, and D. Baltimore.** 1991. B-cell- and myocyte-specific E2-box-binding factors contain E12/E47-like subunits. Mol. Cell. Biol. **11:** 1156–1160.
48. **Mushinski, J. F., W. F. Davidson, and H. C. Morse.** 1987. Activation of cellular oncogenes in human and mouse leukemia-lymphomas: spontaneous and induced oncogene expression in murine B lymphocytic neoplasms. Cancer Invest. **5:**345–368.
49. **Neurath, M. F., E. E. Max, and W. Strober.** 1995. Pax5 (BSAP) regulates the murine immunoglobulin 3′α enhancer by suppressing binding of NF-αP, a protein that controls heavy chain transcription. Proc. Natl. Acad. Sci. USA **92:**5336–5340.
50. **Neurath, M. F., W. Strober, and W. Yoshio.** 1994. The murine Ig 3′ α enhancer is a target site with repressor function for the B-cell lineage-specific transcription factor BSAP (NF-HB, Sα-BP). J. Immunol. **153:**730–742.
51. **Okabe, T., T. Watanabe, and A. Kudo.** 1992. A pre-B and B cell-specific DNA-binding protein, EBB-1, which binds to the promoter of the VpreB1 gene. Eur. J. Immunol. **22:**37–43.
52. **Palacios, R., H. Karasuyama, and A. Rolink.** 1987. $Ly1^+$ pro-B lymphocyte clones. Phenotype, growth requirements, and differentiation in vitro and in vivo. EMBO J. **6:**3687–3693.
53. **Park, K., and M. L. Atchison.** 1991. Isolation of a candidate repressor/activator, NF-E1 (YY1-δ), that binds to the immunoglobulin κ 3′ enhancer and the immunoglobulin heavy-chain μE1 site. Proc. Natl. Acad. Sci. USA **88:**9804–9808.
54. **Pfeifer, G. P., and A. D. Riggs.** 1991. Chromatin differences between active and inactive X chromosomes revealed by genomic footprinting of permeabilized cells using DNase I and ligation-mediated PCR. Genes Dev. **5:**1102–1113.
55. **Pfeifer, G. P., R. L. Tanguay, S. D. Steigerwald, and A. D. Riggs.** 1990. In vivo footprint and methylation analysis by PCR-aided genomic sequencing: comparison of active and inactive X chromosomal DNA at the CpG island and promoter of human PGK-1. Genes Dev. **4:**1277–1287.
56. **Picard, D., and W. Schaffner.** 1984. A lymphocyte-specific enhancer in the mouse immunoglobulin κ gene. Nature (London) **307:**80–82.
57. **Pongubala, J. M. R., and M. L. Atchison.** 1991. Functional characterization of the developmentally controlled immunoglobulin kappa 3′ enhancer: regulation by Id, a repressor of helix-loop-helix transcription factors. Mol. Cell. Biol. **11:**1040–1047.
58. **Pongubala, J. M. R., and M. L. Atchison.** 1995. Activating transcription factor 1 and cyclic AMP response element modulator can modulate the activity of the immunoglobulin κ 3′ enhancer. J. Biol. Chem. **270:**10304–10313.
59. **Pongubala, J. M. R., S. Nagulapalli, M. J. Klemsz, S. R. McKercher, R. A. Maki, and M. L. Atchison.** 1992. PU.1 recruits a second nuclear factor to a site important for immunoglobulin κ 3′ enhancer activity. Mol. Cell. Biol. **12:**368–378.
60. **Queen, C., and D. Baltimore.** 1983. Immunoglobulin gene transcription is activated by downstream sequence elements. Cell **33:**741–748.
61. **Reed, K. C., and D. A. Mann.** 1985. Rapid transfer of DNA from agarose gels to nylon membranes. Nucleic Acids Res. **13:**7207–7221.
62. **Reth, M. G., P. Ammirati, S. Jackson, and F. W. Alt.** 1985. Regulated progression of a cultured pre-B cell line to the B-cell stage. Nature (London) **317:**353–355.
63. **Rolink, A., and F. Melchers.** 1991. Molecular and cellular origins of B lymphocyte diversity. Cell **66:**1081–1094.
64. **Schlissel, M. S., and D. Baltimore.** 1989. Activation of immunoglobulin kappa gene rearrangement correlates with induction of germline kappa gene transcription. Cell **58:**1001–1007.
65. **Sha, W. C., H.-C. Liou, E. I. Tuomanen, and D. Baltimore.** 1995. Targeted disruption of the p50 subunit of NF-κB leads to multifocal defects in immune responses. Cell **80:**321–330.
66. **Singh, M., and B. K. Birshtein.** 1993. NF-HB (BSAP) is a repressor of the murine immunoglobulin heavy-chain 3′ α enhancer at early stages of B-cell differentiation. Mol. Cell. Biol. **13:**3611–3622.
67. **Staudt, L. M., and M. J. Lenardo.** 1991. Immunoglobulin gene transcription. Annu. Rev. Immunol. **9:**373–398.
68. **Sun, X.-H.** 1994. Constitutive expression of the Id1 gene impairs mouse B-cell development. Cell **79:**893–900.
69. **Takeda, S., Y.-R. Zou, H. Bluethmann, D. Kitamura, U. Muller, and K. Rajewsky.** 1993. Deletion of the immunoglobulin κ chain intron enhancer abolishes κ chain gene rearrangement in cis but not λ chain gene rearrangement in trans. EMBO J. **12:**2329–2336.
70. **Travis, A., A. Amsterdam, C. Belanger, and R. Grosschedl.** 1991. LEF-1, a gene encoding a lymphoid-specific protein with an HMG domain regulates

T-cell receptor α enhancer function. Genes Dev. **5:**880–894.
71. **Van Ness, B. G., M. Weigert, C. Coleclough, E. L. Mather, D. E. Kelley, and R. P. Perry.** 1981. Transcription of the unrearranged mouse Cκ locus: sequence of the initiation region and comparison of activity with a rearranged Vκ-Cκ gene. Cell **27:**593–602.
72. **Wallrath, L. L., Q. Lu, H. Granok, and S. C. R. Elgin.** 1994. Architectural variations of inducible eukaryotic promoters: preset and remodeling chromatin structures. Bioessays **16:**165–169.
73. **Weih, F., D. Carrasco, S. K. Durham, D. S. Barton, C. A. Rizzo, R.-P. Ryseck, S. A. Lira, and R. Bravo.** 1995. Multiorgan inflammation and hematopoietic abnormalities in mice with a targeted disruption of relB, a member of the NF-κB/Rel family. Cell **80:**331–340.
74. **Wilson, R. B., M. Kiledjian, C.-P. Shen, R. Benezra, P. Zwollo, S. M. Dymecki, S. V. Desiderio, and T. Kadesch.** 1991. Repression of immunoglobulin enhancers by the helix-loop-helix protein Id: implications for B-lymphoid-cell development. Mol. Cell. Biol. **11:**6185–6191.
75. **Wu, C.** 1980. The 5′ ends of Drosophila heat shock genes in chromatin are hypersensitive to DNase I. Nature (London) **286:**854–860.
76. **Yancopoulos, G. D., and F. W. Alt.** 1985. Developmentally controlled and tissue-specific expression of unrearranged V_H gene segments. Cell **40:**271–281.
77. **Yuan, D., and P. W. Tucker.** 1984. Transcriptional regulation of the μ-δ heavy chain locus in normal murine B lymphocytes. J. Exp. Med. **160:**564–583.
78. **Zhang, L., and J. D. Gralla.** 1989. In situ nucleoprotein structure at the SV40 major late promoter: melted and wrapped DNA flank the start site. Genes Dev. **3:**1814–1822.
79. **Zhuang, Y., P. Soriano, and H. Weintraub.** 1994. The helix-loop-helix gene E2A is required for B-cell formation. Cell **79:**875–884.